Dissertation for the degree of Doctor of Philosophy

A Study on the Preliminary Design and Performance Analysis of Radial Outflow Turbines for a Supercritical Carbon Dioxide Power Cycle and an Organic Rankine Cycle

Supervisor Prof. You-Taek Kim

February 2020

Department of Convergence Study on the Ocean Science and Technology
Ocean Science and Technology School
Korea Maritime and Ocean University

Jun-Seong Kim

The dissertation for the degree of Doctor of Philosophy by Jun-Seong Kim has been approved by the committee members.

Chair	Ph.D.	Tae-Woo Lim	
Member	Ph.D.	Do-Yeop Kim	
Member	Ph.D.	Chang-Hyo Son	
Member	Ph.D.	Jin-Hak Yi	
Member	Ph.D.	You-Taek Kim	

December 18, 2019

Ocean Science and Technology School

Korea Maritime and Ocean University

Table of Contents

List of Tables

List of Tables

List of Figures

List of Figures

List of Figures

Nomenclature

A	area [m^2]
C	absolute velocity [m/s]
c	true chord length [mm]
C_0	spouting velocity [m/s]
C_L	lift coefficient
f	correction coefficient
H	height [mm]
h	enthalpy [J/kg]
K	loss coefficient
k	specific heat ratio
M	Mach number, mass flow rate ratio
$\dot{m}$	mass flow rate [kg/s]
N_s	specific speed
P	pressure [MPa]
PR	pressure ratio
$\dot{Q}$	volume flow rate [m^3/s]
R	gas constant [J/mol·K]
r	radius [mm]
Re	Reynolds number
s	entropy [J/kg·K], pitch [mm]
T	temperature [K]
TR	temperature ratio
U	peripheral velocity [m/s]
V	specific volume [m^3/kg]
W	relative velocity [m/s]
$\dot{W}$	power

Greeks

α	absolute flow angle [°]
β	relative flow angle [°]
η	efficiency [%]
ν	velocity ratio
ρ	density [kg/m^3]
ϕ	flow coefficient
ψ	loading coefficient
ω	angular velocity [rad/s]

Subscripts

0	total state
00	total state at station 0
1	nozzle inlet
2	nozzle exit & rotor inlet
3	rotor exit
$accel$	accelerating
AS	aspect ratio
b	blade
c	critical point parameter
m	meridional component
N	nozzle
P	profile
R	rotor
r	relative
Re	Reynolds number
ref	reference value
s	isentropic
Sec	secondary
sh	shock
ts	total to static
tt	total to total
θ	tangential component

초임계 이산화탄소 발전 사이클과 유기 랭킨 사이클용 외향 반경류 터빈의 예비설계 및 성능분석에 관한 연구

김 준 성

한국해양대학교 해양과학기술전문대학원
해양과학기술융합학과

초 록

최근 지구온난화 및 환경오염에 대한 경각심이 더욱 커지며, 점진적으로 환경규제를 강화하고 있다. 또한, 환경문제의 원인이 되는 고전적인 발전 시스템을 대체할 수 있는 방안에 대하여 전 세계적으로 주목하고 있다. 초임계 이산화탄소 발전 사이클과 유기 랭킨 사이클은 이러한 세계적인 경향에 적합한 친환경 발전 사이클이다. 한편, 터빈은 발전 사이클의 효율에 있어 지대한 영향을 미치는 요소이다. 근래 이러한 발전 사이클의 터빈으로 외향 반경류 터빈에 대한 관심이 커지고 있다. 외향 반경류 터빈은 설계와 제작에 있어 축류 터빈보다 용이하고, 고출력이 요구되는 설계조건에 있어 내향 반경류 터빈보다 유리하다.

외향 반경류 터빈이 지닌 다양한 장점으로 인하여, 일부 연구기관에서는 친환경 발전 사이클용 외향 반경류 터빈의 설계기법에 관한 연구를 수행하고 있다. 그러나 기존의 연구에서는 터빈의 예비설계단계에서 목표 효율이 불분명하다. 설계된 터빈의 효율이 열역학적 사이클에서 고려된 터빈의 효율과 상이할 시, 사이클은 설계된 터빈의 효율을 고려하여 재설계되어야 한다. 그러므로 터빈의 예비설계단계에서 목표효율을 분명히 하고, 설계된 터빈은 목표효율을 충족할 필요가 있다.

본 연구에서는 독창적인 알고리즘을 이용하여 외향 반경류 터빈의 예비설계 프로그램을 개발하였으며, 대표적인 특징은 다음과 같다. 우선, 목표효율을 프로그램의 입력변수로 사용함으로써 열역학적 사이클에서 요구하는 효율에 근접하도록 터빈을 설계할 수 있다. 또한, 터빈의 주요형상을 결정하고, 효율에 큰 영향을 미치는 노즐 출구의 상태량을 정확하게 예측하기 위하여 압력손실모델을 이용하였다. 그리고 효율적이고 용이하게 터빈을 설계하도록 알고리즘을 구성하였다. 마지막으로 오직 하나의 변수에 대하여 반복계산을 수행함으로써 빠른 시간 내 터빈의 설계가 가능하다.

개발한 예비설계 프로그램을 활용하여 초임계 이산화탄소 발전 사이클과 유기 랭킨 사이클용 외향 반경류 터빈의 설계를 수행하였다. 예비설계 프로그램에서 제시한 터빈의 초기형상은 설계조건을 다소 만족하지 못하였으나, 깃의 편향각이 터빈의 성능에 있어 지대하게 영향을 미치는 중요변수임을 밝혔다. 본 연구에서는 터빈의 초기 형상에 대하여 체계적이고 용이한 최적화 기법을 제시하였다. 예비설계 프로그램에서 제시한 터빈의 초기형상은 최적화 기법을 통하여 각 사이클의 설계조건을 만족하는 외향 반경류 터빈을 설계할 수 있었다.

설계된 외향 반경류 터빈은 다양한 작동조건에 따른 탈설계 성능분석이 수행되었다. 그 결과, 각 터빈의 회전수에서 터빈의 입구온도, 질량유량 및 압력비가 상승할수록 터빈의 출력이 증가하는 결과를 얻을 수 있었다. 또한, 설계 회전수에 근접하도록 터빈을 작동하는 것이 터빈의 성능에 유리하다는 결과를 얻었다. 각 사이클의 터빈은 독립변수들의 변화에 따라 출력 및 효율에 있어 대체적으로 유사한 경향을 보였다. 한편, 외향 반경류 터빈은 초임계 이산화탄소보다 유기냉매를 사용할 때 운전조건의 변화에 따라 민감하게 효율이 변화하는 결과를 보였다.

외향 반경류 터빈의 탈설계 성능분석결과를 활용하여 비속도, 부하계수 및 유량계수에 따른 성능곡선을 제시하였다. 본 연구에서 제시한 성능곡선을 통하여 초임계 이산화탄소 및 R143a용 외향 반경류 터빈은 비속도, 부하계수 및 유량계수에 따라 효율예측이 가능하다. 상기 무차원 변수에 따른 성능곡선에서 고효율 및 저효율 지점을 지정한 뒤, CFD 수치해석결과를 분석하였다. 그 결과, 로터 깃의 압력분포, 정체점의 위치 및 입사각 등이 외향 반경류 터빈의 효율에 영향을 미치는 요소임을 밝혔다.

한편, 외향 반경류 터빈은 작동유체에 따라 성능곡선이 상이할 뿐만 아니라, 고효율을 기대할 수 있는 무차원 변수의 범위가 다르다. 그러나 본 연구에서는 각 터빈의 성능곡선에서 공통적으로 고효율에 해당하는 무차원 변수의 범위를 발견할 수 있었다. 즉, 고효율이 요구되는 외향 반경류 터빈의 최적설계 시에 범용적으로 사용할 수 있는 무차원 변수의 범위를 본 연구에서 제안하였다.

본 연구에서 밝힌 연구결과들은 지속적으로 향상될 외향 반경류 터빈 설계기술의 초석이 될 것으로 기대된다. 추후 외향 반경류 터빈의 예비설계 프로그램 및 성분분석에 대한 연구가 꾸준히 이루어진다면, 본 연구에서 개발한 터빈의 설계기술이 초임계 이산화탄소 발전 사이클과 유기 랭킨 사이클 분야에 점진적으로 자리매김할 수 있을 것으로 기대된다.

KEY WORDS: Radial outflow turbine 외향 반경류 터빈; Supercritical carbon dioxide power cycle 초임계 이산화탄소 발전 사이클; Organic Rankine cycle 유기 랭킨 사이클; Preliminary design 예비설계; Performance analysis 성능분석

Chapter 1. Introduction

1.1 Radial outflow turbine

The history of radial outflow turbines begins with Parsons and Ljungström turbines.

In 1884, Parsons tried to create multi-stage axial turbines that were highly efficient and developed his first steam turbines. In 1889, he was unable to use multi-stage axial turbines due to a legal dispute. Since then, he has researched and developed radial outflow turbines as an alternative to multi-stage axial turbines. The turbines developed by Parsons have been used in power industries and a engine of a ship called “Turbinia” (Fig. 1). Thus, Parsons inability to use multi-stage axial turbines leads to the development of radial outflow turbines that could be used for power generation and ship propulsion (Meher-Homji, 2000; Spadacini & Rizzi, 2017).

In 1908, the Ljungström turbines were developed by Swedish engineers, the Birger and Fredrik Ljungström brothers. The turbines were produced in STAL (Svenska Turbinfabriks Aktiebolaget Ljungström), established in 1913. The Ljungström turbines have unique features called multi-stage counter-rotating centrifugal steam turbines. The turbines, shown in Fig. 2, consist of two disks facing each other, and are connected by two independent shafts. The working fluid enters the center through ports and slots and flows radially through the counter-rotating blades of the two discs. This turbine was used in various fields such as power generation (Spadacini & Rizzi, 2017).

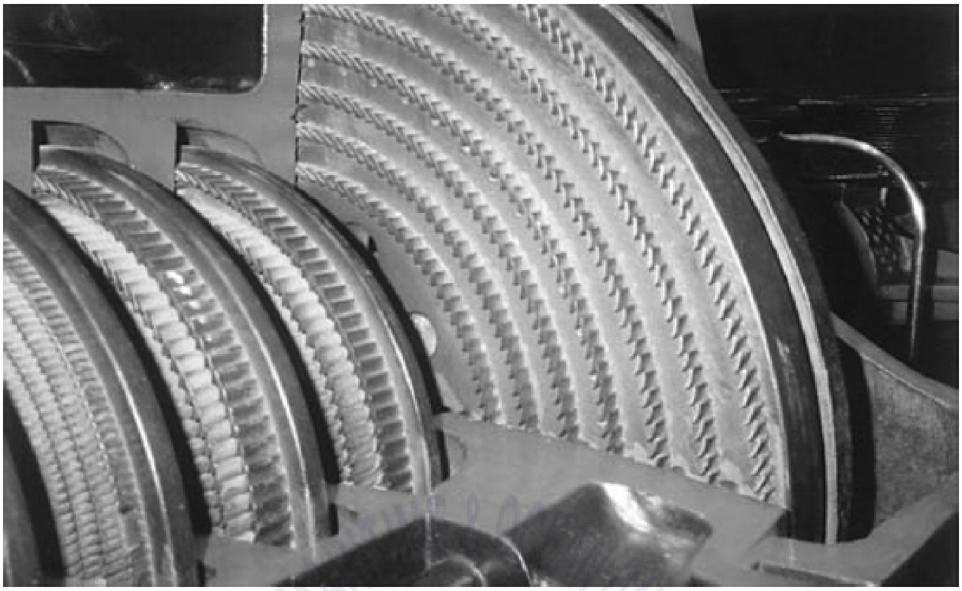

Fig. 1 A radial outflow Parsons turbine (Meher-Homji, 2000; Spadacini & Rizzi, 2017)

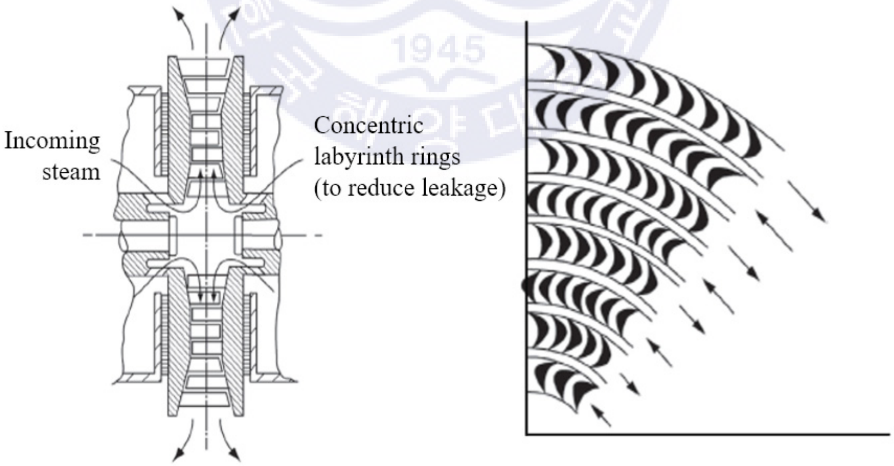

Fig. 2 Schematic drawing of a Ljungström turbine (Dixon, 1998; Spadacini & Rizzi, 2017)

Recently, Italian turbine maker EXERGY has developed a radial outflow turbine for geothermal power plants by applying Ljungström turbines for commercial purposes (Fig. 3). EXERGY advertised the features and expected advantages of radial outflow turbines when compared to conventional turbines (Spadacini et al, 2015). As such, radial outflow turbines are receiving attention from the power generation industry.

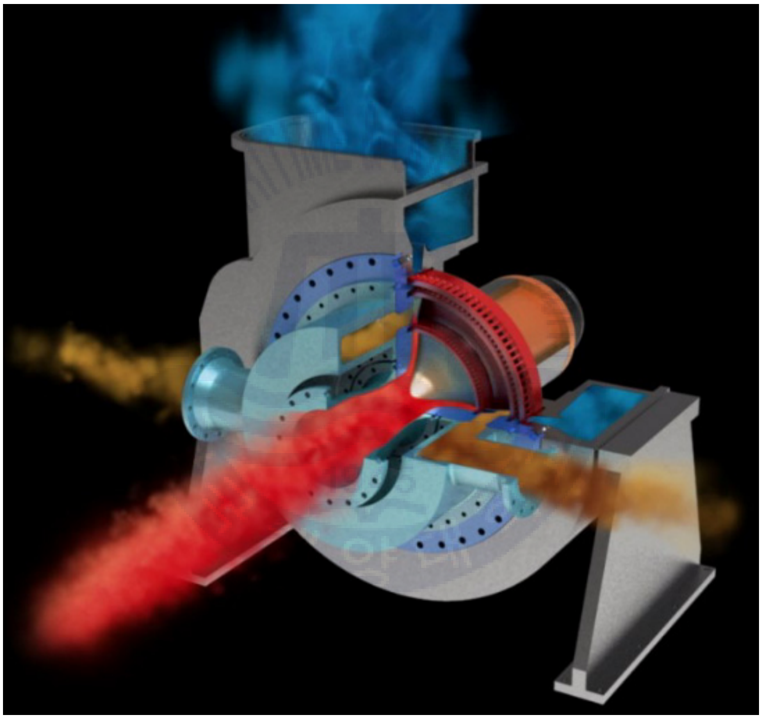

Fig. 3 A radial outflow turbine made by EXERGY (Spadacini et al., 2015)

When mechanical energy is utilized during the power generation cycle, the appropriate type of expander should be used depending on the operating conditions. In general, the expander is divided into a volume expander and a turbo expander. The volume expander has no risk of breakage by droplets but has the disadvantage of relatively low efficiency. On the other hand, the turbo expander is very vulnerable to two-phase working fluids but is suitable for relatively high capacity and efficiency purposes (Bao & Zhao, 2013). If the working fluid entering the expander can be prevented from becoming two-phase during the expansion process, it is advantageous to select a turbo expander for efficiency (Kim et al., 2019a).

The most widely used types of turbines are mainly axial turbines and radial inflow turbines, each of which has distinct characteristics. Axial turbines are advantageous at high flow rates. Additionally, high efficiency and output can be expected by constructing this turbine in multiple stages (Wang et al., 2018). Radial inflow turbines are suitable for low flow rates, are easy to fabricate, and perform well under off-design conditions (Bao & Zhao, 2013). However, in the axial turbine, the blade height increases from the first stage to the last stage as the working fluid expands (Spadacini & Rizzi, 2017). Therefore, when approaching the last stage, the blade shows increased difference in the velocity triangle between the hub and tip. This is difficult to manufacture as the blades have to be twisted (Spadacini & Rizzi, 2017; Wang et al., 2018). Radial inflow turbines generally consist of only one stage and are difficult to use in cycles requiring high pressure ratios owing to their Mach number limitation (Al Jubori et al., 2017a).

Radial outflow turbines can be used to compensate for the shortcomings of axial and radial inflow turbines. Fig. 4 shows the structure of a typical radial outflow turbine (Spadacini et al., 2015). Radial outflow turbines, also referred to as centrifugal turbines, expand radially after the working fluid enters the axial direction.

Radial outflow turbines typically have the following advantages (Luo et al., 2017; Wang et al., 2018).

(1) As the radius of the flow area increases with the specific volume of the working fluid in the expansion process, it is possible to design the change in blade height to be small or constant.

(2) The peripheral velocity is constant according to the span of the blade, and the velocity triangle between the hub and tip is constant so that the blade does not have to be twisted.

(3) Since multi-stage configuration is easy, there is no restriction on the pressure ratio, enabling its use for cycles requiring high power.

In other words, radial outflow turbines are easier to design and produce compared to axial turbines. Their multi-stage configurations also ensure a higher output response than radial inflow turbines.

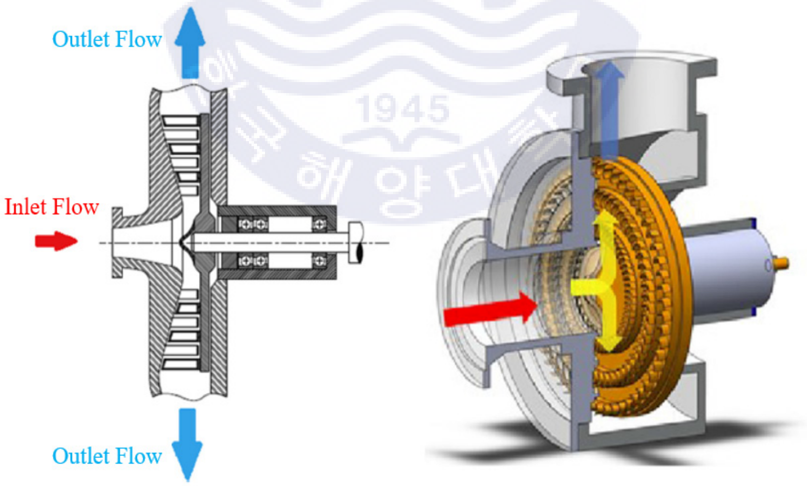

Fig. 4 Conventional structure of a radial outflow turbine (Spadacini et al., 2015)

1.2 Research background

Environmental regulations are being tightened around the world due to air pollution and global warming problems. As a result, there is increasing research effort on power generation systems that can replace fossil fuels. To cope with the regulations that are being enforced by these global trends, eco-friendly power cycles such as supercritical carbon dioxide (sCO_2) power cycle and organic Rankine cycle (ORC) are receiving research and commercial attention.

The supercritical CO_2 power cycle uses the CO_2 of supercritical state as the working fluid. Supercritical CO_2 has high heat capacity, excellent fluidity, and a higher density than gas, making it possible to miniaturize equipment (Luo et al., 2017). It is also an economical, safe, and highly effective natural working fluid in the supercritical state (Kim et al., 2018). Supercritical CO_2 power cycle can be composed of Brayton cycle and Rankine cycle depending on the purpose of use and operating conditions as shown in Fig. 5.

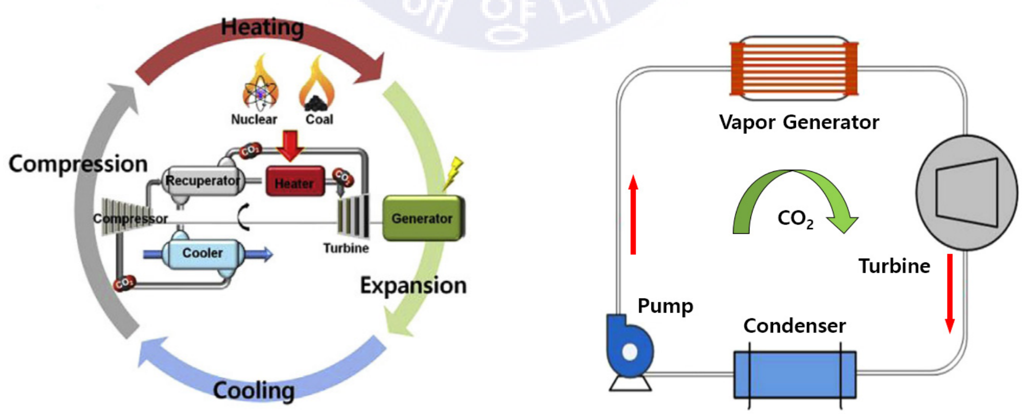

Fig. 5 Brayton cycle and Rankine cycle using supercritical carbon dioxide (Ahn et al., 2015; Sarkar, 2015)

Here, the cycle in which the CO_2 in the supercritical state exceeds the critical pressure in the whole process is called a supercritical cycle. In addition, the pressure during the expansion process decreases below the critical pressure, and the cycle required for the condensation process is defined as a transcritical cycle (Kim et al., 2012).

Because of the various advantages of supercritical CO_2, research on the supercritical CO_2 power generation cycle has been actively conducted recently. Zhang et al. (2005) conducted an experimental study on the Rankine cycle, which recovers solar energy using supercritical CO_2, and presented positive possibilities for thermodynamic efficiency. Cayer et al. (2009) analyzed the transcritical CO_2 cycle through energy analysis, exergy analysis, finite size thermodynamics analysis and calculation of the heat exchangers' surface. Wang et al. (2010) analyzed the performance of supercritical CO_2 power generation cycle using genetic algorithm and artificial neural networks. Kim et al. (2012) presents thermodynamic analysis of various supercritical and transcritical CO_2 cycles depending on the low and high temperature heat sources. Sarkar (2015) commented on the supercritical Rankine cycle for various heat sources and working fluids, arguing that it would be advantageous to use CO_2 as the working fluid, and positively assessed the prospects for the supercritical CO_2 Rankine cycle. Ahn et al. (2015) summarized the application of the supercritical CO_2 power cycle according to various heat sources such as nuclear, fossil fuel, waste heat, and renewable energy. After classifying various layouts that can be applied to each heat source, the performance of each layout was compared and analyzed. In recent years, research has been conducted on a supercritical CO_2 power generation cycle on a ship. Choi (2016) conducted a thermodynamic analysis of a two-stage reheated transcritical CO_2 power generation system using waste heat generated from internal combustion engines for 6,800 TEU container ships. Sharma et al. (2017) constructed supercritical CO_2 regenerative recompression Brayton cycle using waste heat from a marine gas turbine engine, and then performed optimization and performance analysis.

Studies on the experiment and turbo machines of supercritical CO_2 power cycles are also ongoing. Iverson et al. (2013) conducted an experimental study to identify the operating conditions in abnormal circumstances for the prototype solar-thermal power plant based on the supercritical CO_2 Brayton cycle. In addition, Cho et al. (2016) conducted experimental studies of supercritical CO_2 power cycles through the establishment of test loops of 10 kW class. The above papers are characterized by the application of a turbo-alternator-compressor type turbomachinery in which a radial inflow turbine, an alternator and a centrifugal compressor are coaxially operated. Fuller et al. (2012) sought to familiarize cycle designers and turbomachine designers with regards to supercritical CO_2 cycles by providing guidelines for turbomachinery based on cycle conditions. Odabaee et al. (2016) conducted a design and CFD analysis of a radial inflow turbine for a 100 kW supercritical CO_2 power cycle using a real gas equation of estate and real gas property files. Lee et al. (2012) developed a preliminary design program for axial compressors and turbines, and radial compressors and turbines that make up the supercritical CO_2 Brayton cycle. This program uses a mathematical design model and a loss model to present shape information and off-design performance of each fluid machine according to operating conditions. As such, supercritical CO_2 cycles are continuously being studied through cycle analysis, component design, and experimental studies.

Meanwhile, Tartière and Astolfi (2017) summarized the global status of the organic Rankine cycle market by company and heat source. They forecast that the organic Rankine cycle market would continue to grow. The organic Rankine cycle utilizes hydrocarbon compounds or organic refrigerants that have a much lower boiling point than water. The working fluid can be boiled in a high pressure gas state using a low temperature heat source (Tchanche et al., 2011). In classical power generation cycles, energy cannot be recovered from low temperature heat sources for economic reasons (Kim et al., 2019a). However, the organic Rankine cycle makes it possible to recover energy from low temperature heat sources such as biomass, ocean, industrial waste heat and geothermal solar heat (Tchanche et al., 2014). The need for the organic Rankine cycle is highlighted in various energy industries, and research and commercialization are ongoing.

The basic composition of the organic Rankine cycle is shown in Fig. 6 (Kim et al., 2019b). Representative factors that determine the efficiency of the organic Rankine cycle include the turbine, working fluid and cycle configuration. Among them, the turbine is relatively more important in the efficiency and cost of the organic Rankine cycle (Bao & Zhao, 2013). Accordingly, there continues to be various research findings on the turbine design technology for the organic Rankine cycle.

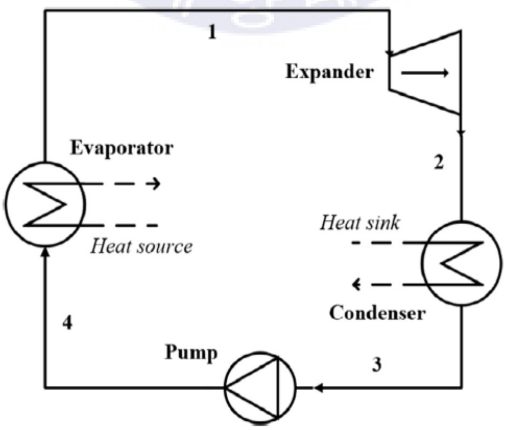

Fig. 6 Schematic diagram of an organic Rankine cycle (Kim et al., 2019b)

Kang (2012) designed a radial inflow turbine for organic Rankine cycles using R245fa as a working fluid, and then carried out an experimental study. As a result, the maximum average cycle efficiency, turbine efficiency and power were achieved at 5.22 %, 78.7 % and 32.7 kW, respectively. Da Lio et al. (2014) optimally designed single stage axial turbines for organic Rankine cycles using real fluid properties and recent loss models. In addition, the performance chart according to various dimensionless variables is presented to find the optimum design point of axial turbines for the organic Rankine cycle system. Al Jubori et al. (2016) designed micro-scale axial and radial inflow turbines for the organic Rankine cycle using R141b, R1234yf, R245fa, n-butane and n-pentane. Here, the performance of each turbine was analyzed according to the type of working fluid and turbine through the preliminary design and CFD results. Sauret and Rowlands (2011) studied the organic Rankine cycle for geothermal power generation. They designed the radial inflow turbines using the Concepts NREC RITAL. Following this, performance analysis of the turbines was conducted according to various working fluids. Sauret and Gu (2014) designed a 400 kW radial inflow turbine using R143a with reference to Sauret and Rowlands (2011). Through the off-design analysis of the turbine using CFD, they presented the performance curve of the radial inflow turbine for geothermal power generation. Do-Yeop Kim and You-Taek Kim (2017a) conducted a study on the design of a 200 kW radial inflow turbine for ocean thermal energy conversion. In this study, a preliminary design technique using loading and flow coefficients that meet the target efficiency was developed. The CFD verification results were satisfactory and produced performance curves according to off-design conditions.

Do-Yeop Kim and You-Taek Kim (2017b) developed their own Radial Turbine Design Modeler (RTDM) that presents rational turbine geometry using operating conditions without using gas turbine performance charts and ideal gas equations. As a result, the RTDM turbine showed better performance than the turbine designed by Sauret and Gu (2014). In addition, Kim et al. (2019b) constructed experimental equipment as shown in Fig. 7 to compare and analyze the performance of turbines designed using RTDM and RITAL. They found that the two turbines were similar in term of power and efficiency. Kim et al. (2019b) also undertook further research on the model predicting turbine performance by integrating deep neural networks with experimental results. This breadth of research on axial turbines and radial inflow turbines for organic Rankine cycles demonstrated that these turbines have been investigated in a variety of ways, including preliminary design techniques, CFD analysis, and experimentally.

Fig. 7 Photograph of the experimental equipment for an organic Rankine cycle (Kim et al., 2019b)

Supercritical CO_2 power cycles and organic Rankine cycles are being studied and developed in many research institutes and industries. However, the research on the radial outflow turbine as an expander of the cycles is relatively scant. Meanwhile, because radial outflow turbines can take advantage of traditional axial and radial inflow turbines, interest in these turbines has been increasing as a supercritical CO_2 power cycle turbine and an organic Rankine cycle turbine. Some research institutes have now advanced research on radial outflow turbines.

A representative research institute for radial outflow turbines is the Fluid Dynamics of Turbomachines Laboratory at the Polytechnic University of Milan in collaboration with the Italian company EXERGY (Wang et al., 2018). From this research institute, Persico et al. (2013) presented a unique design technique for the radial outflow turbine of a 1 MW organic Rankine cycle, and analyzed the performance of the turbine through CFD. Pini et al. (2013) designed radial outflow turbines for organic Rankine cycles consisting of three and six stages. The optimal design was aimed at achieving the same output for both turbines, and 1D and CFD results were compared and analyzed. Casati et al. (2014) studied radial outflow turbines for a 10 kW organic Rankine cycle and suggested the possibility of radial outflow turbines in a mini organic Rankine cycle. Persico et al. (2015) used CFD to analyze the blade-to-blade and secondary flow patterns seen in the stator and rotor of radial outflow turbines. Persico et al. (2017, 2018) also presented their own code and demonstrated optimization techniques for the blade shape of radial outflow turbines. Moreover, they compared the baseline and optimal configuration of the blades, revealing various advantages of the optimization.

The University of Shanghai for Science and Technology in China has also conducted numerous studies on radial outflow turbines. Luo et al. (2017) designed a radial outflow turbine for a supercritical CO_2 power cycle. The blade shape was optimized until the output and efficiency of the turbine presented by CFD were satisfied, and off-design analysis of the final shape was performed. Luo et al. (2018) designed a three-stage radial outflow turbine based on the design conditions of a four-stage axial turbine. Following this, they conducted a CFD verification and off-design analysis. Song et al. (2017) analyzed organic Rankine cycles for various working fluids, and then designed and optimized radial outflow turbines using R123 as a working fluid from one to three stages. Wang et al. (2018) demonstrated guide vane and volute design techniques for radial outflow turbines, and then analyzed the performance of radial outflow turbines for various volute configurations. In addition, Wang et al. (2019) and Liu and Huang (2019) designed radial outflow turbines using R245fa and R141b as the working fluid, respectively. Both studies were characterized by the design of single-stage transonic turbines for high-pressure organic Rankine cycles.

On top of these studies, Al Jubori et al. (2017a) designed an axial turbine and a radial outflow turbine for the organic Rankine cycle, and carried out validations and comparative analyses of the preliminary design through CFD. Al Jubori et al. (2017b) also designed axial turbines, radial inflow turbines, and radial outflow turbines for organic Rankine cycles. They verified and compared them through CFD in a manner similar to previous studies and presented new performance maps for various turbine types. Maksiuta et al. (2017) studied radial outflow turbines for a 3 MW waste heat recovery organic Rankine cycle, and proposed a unique preliminary design technique for multi-stage radial outflow turbines with different enthalpy drops in each stage.

As such, the radial outflow turbine complements the limitations of existing turbines in various power cycle fields and has the potential to be highly efficiency. However, the preliminary design technique for the radial outflow turbine in existing studies focused only on the maximum efficiency of the turbine, the target efficiency being unclear. When the efficiency of a turbine differs from that considered in the thermodynamic cycle, an inefficient case arises where the cycle has to be re-designed to take the turbine efficiency into account. Therefore, it is important to clarify the target efficiency during the preliminary design step of the turbine, and the designed turbine must meet this target (Do-Yeop Kim & You-Taek Kim, 2017a).

The preliminary design refers to the process of determining the geometric shape of the machine using only the operating conditions. The performance of the shape presented in the preliminary design step must be analyzed using numerical analysis such as CFD. This is because it is very difficult for the initial shape obtained from the preliminary design to meet the design goal at once. If necessary, the shape of the machine should be improved through strict performance prediction. In other words, the preliminary design involves presenting a shape, which is the basis for the final shape that satisfies the target performance. A highly accurate preliminary design simplifies the design process of the machine.

The process of improving the shape to satisfy the design goal of the machine is expressed as optimization. A shape optimization process is necessary even in the design of radial outflow turbines. This was the case in Luo et al. (2017, 2018) and Song et al. (2017), where CFD was conducted on the initial shape presented in the preliminary design, and then the blade shape was optimized based on the results. These findings demonstrate that the optimization process for determining the final shape through numerical analysis prior to the experiment is a conventional process in the design of a radial outflow turbine.

Optimally designed turbines must be numerically analyzed for off-design conditions. It is necessary to understand the performance of turbines outside the design point through off-design analysis based on changes to different variables. In addition, off-design performance results can be used as data for performance curves according to dimensionless variables that are not limited to specific operating conditions.

Meanwhile, Sayers (1990) notes that it is necessary to reduce the number of key variables that affect the performance of turbomachines by grouping them into dimensionless variables. Sayers (1990) mentioned that the performance curve according to dimensionless variables can be applied to the same class of machines provided that the similarity law is satisfied. And then, the performance curve of turbomachinery according to dimensionless specific speed was presented. The specific speed does not use variables related to the shape of the turbine, but is a dimensionless variable consisting only of operating conditions (Aungier, 2006; Moustapha et al., 2003).

Moustapha et al. (2003) introduced the Smith chart that can predict the stage efficiency of turbines using the loading and flow coefficients. Multiple studies have verified the Smith chart, and suggested suitable loading and flow coefficients for preliminary design of the turbine. Spadacini and Rizzi (2017) compared the performance of a radial outflow turbine and an axial turbine using the Smith chart as a design method. They found that even with radial outflow turbines, the loading and flow coefficients of the blades can have significant influence on turbine efficiency.

Therefore, to establish the optimum design criteria for radial outflow turbines, it is advantageous to understand the relationship between these dimensionless variables and turbine performance. In doing this, the performance curve of the radial outflow turbine must be established to find the optimum range of dimensionless variables that can be used universally.

1.3 Research objective

This study performs the preliminary design and performance analysis of radial outflow turbines for a supercritical CO_2 power cycle and an organic Rankine cycle. The main research objectives are described below.

First, I study the preliminary design program for radial outflow turbines using the target efficiency as an input variable. This is to improve issues with the existing preliminary design techniques of radial outflow turbines where target efficiency is unclear. I propose a unique algorithm to meet the target performance of the radial outflow turbine by considering the design models suitable for the preliminary design.

Second, I design radial outflow turbines for a supercritical CO_2 power cycle and an organic Rankine cycle through the preliminary design program. After selecting the design conditions of the turbine required for the thermodynamic cycle, a case study is conducted for each cycle. CFD analysis is performed to verify the preliminary design program. The results are used to identify the critical variable in the design of the radial outflow turbine. The turbines are designed to meet design goals through optimization.

Third, I implement an off-design analysis on the designed turbine according to the turbine inlet temperature, mass flow rate, pressure ratio and rotational speed. The analysis enables the identification of the trends of power output and efficiency of radial outflow turbines according to each independent variable. In addition, the off-design performance results seen in each cycle turbine are compared and analyzed.

Fourth, using the data output from off-design performance analysis, I develop performance curves of the radial outflow turbine according to specific speed, loading and flow coefficients. After selecting the high and low efficiency points from the performance curves, the CFD numerical analysis results are analyzed to identify factors that affect the efficiency of the turbine.

Finally, I identify the range of specific speed, loading and flow coefficients for a radial outflow turbine that apply for high efficiency in each cycle. I also propose the optimal range of dimensionless variables that can be used universally for radial outflow turbines.

The overall research aim of this study is to secure the unique design technology of the radial outflow turbine for supercritical CO_2 power cycles and organic Rankine cycles.

Chapter 2. Preliminary design of radial outflow turbines

2.1 Basic theory

Basic theories and concepts necessary for the preliminary design and performance analysis of radial outflow turbines are described in this section. The velocity triangles and blading terminology of the radial outflow turbine are illustrated in Figs. 8-9. The h-s diagram of the turbine is shown in Fig. 10.

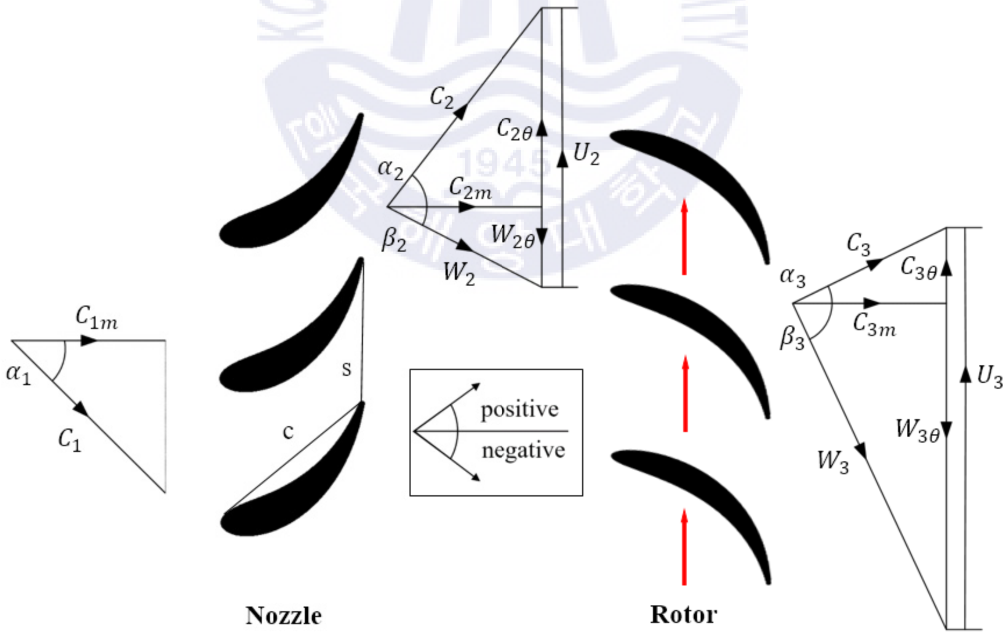

Fig. 8 Schematic diagram of velocity triangles for a radial outflow turbine

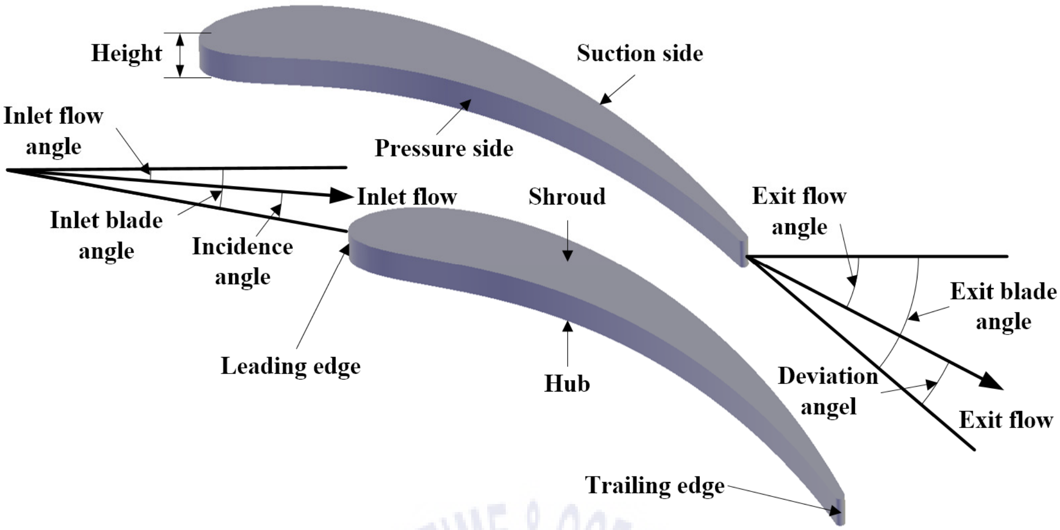

Fig. 9 Blading terminology of a radial outflow turbine

The specific power of the turbine can be defined as Eq. (1) with total enthalpy drop and a Euler equation (Sayers, 1990). A distinctive feature of radial outflow turbines, as opposed to axial turbines, is that there is a difference in the peripheral velocity of the rotor inlet and outlet. That is, for radial outflow turbines, it is necessary to actively minimize the tangential absolute velocity of the rotor outlet ($C_{3\theta}$), which impedes the specific power. The mass flow rate of Eq. (1) is equal to Eq. (2). Here, if the meridian (radius) absolute velocity is constant, then the mass flow rate at each point can be considered only for density and flow area.

$$\dot{W} = \dot{m}(h_{01} - h_{03}) = \dot{m}(U_2 C_{2\theta} - U_3 C_{3\theta}) \tag{1}$$

$$\dot{m} = \rho_1 C_{1m} 2\pi r_1 H = \rho_2 C_{2m} 2\pi r_2 H = \rho_3 C_{3m} 2\pi r_3 H \tag{2}$$

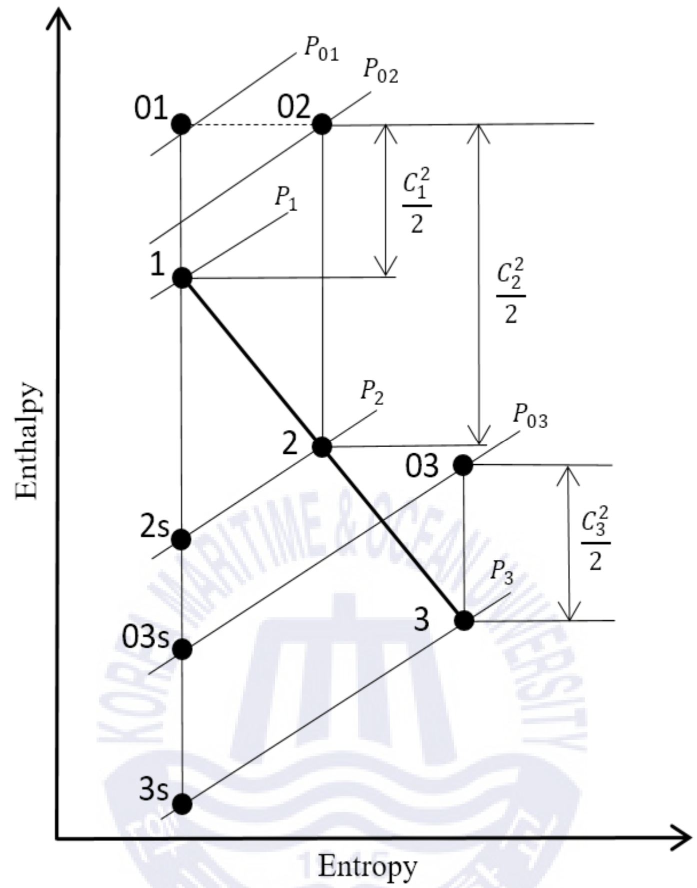

Fig. 10 h-s diagram of working fluids in a radial outflow turbine

The total-to-total efficiency (η_{tt}) and total-to-static efficiency (η_{ts}) of the turbine in Fig. 10 may be quantified using Eqs. (3)–(4), respectively. In addition, the relationship between the total state enthalpy (h_0) and static state enthalpy (h) at a specific point is shown by Eq. (5).

$$\eta_{tt} = \frac{h_{01} - h_{03}}{h_{01} - h_{03s}} \tag{3}$$

$$\eta_{ts} = \frac{h_{01} - h_{03}}{h_{01} - h_{3s}} \tag{4}$$

$$h_0 = h + \frac{1}{2}C^2 \tag{5}$$

Maksiuta et al. (2017) found that radial outflow turbines, as well as radial inflow turbines, had an appropriate velocity ratio (ν) of 0.7. The velocity ratio is defined in Eq. (6). The peripheral velocity of the rotor inlet (U_2) and spouting velocity (C_0) are shown in Eqs. (7)–(8), respectively. The peripheral velocity of the rotor inlet can be determined through the velocity ratio and the spouting velocity. It is possible to determine the radius of the rotor inlet (r_2) using the angular velocity (ω).

$$\nu = U_2 / C_0 \tag{6}$$

$$U_2 = r_2 \omega \tag{7}$$

$$C_0 = \sqrt{2(h_{01} - h_{3s})} \tag{8}$$

The specific speed (N_s) of the turbine is represented by Eqs. (9)–(10) (Aungier, 2006). The specific speed can be calculated using the angular velocity of the turbine, volumetric flow rate at the rotor outlet, and ideal enthalpy drop.

$$N_s = \frac{\omega \sqrt{\dot{Q}_{03}}}{(h_{01} - h_{3s})^{0.75}} \tag{9}$$

$$\dot{Q}_{03} = \dot{m}/\rho_{03} \tag{10}$$

The definitions of the loading coefficient (ψ) and flow coefficient (ϕ) for radial outflow turbines are described in Eqs. (11)–(12). The loading coefficient can be simply expressed as the right side of Eq. (11) if the tangential absolute velocity component of the rotor exit ($C_{3\theta}$) is zero (Moustapha et al., 2003; Spadacini and Rizzi, 2017).

$$\psi = \frac{U_2 C_{2\theta} - U_3 C_{3\theta}}{U_2^2} \simeq \frac{C_{2\theta}}{U_2} \tag{11}$$

$$\phi = \frac{C_{3m}}{U_2} \tag{12}$$

Rothalpy should be preserved in the rotor flow of a turbomachinery. The rothalpy of a radial outflow turbine has the same relationship as Eq. (13).

$$h_2 + \frac{W_2^2}{2} - \frac{U_2^2}{2} = h_3 + \frac{W_3^2}{2} - \frac{U_3^2}{2} \tag{13}$$

2.2 Algorithm of preliminary design

In a few research results on radial outflow turbines, it is worth paying attention to the research of Al Jubori et al. (2017a). The study pointed out the absence of a clear design theory for radial outflow turbines. In addition, his research team designed a radial outflow turbine using a pressure loss model of the axial turbine. By verifying the design algorithm using CFD, they demonstrated that the pressure loss model of the axial turbine was also effective for the design of a radial outflow turbine. Each pressure loss coefficient of the nozzle (K_N, Eq. (14)) and rotor (K_R, Eq. (15)) has a relationship between the total-to-total efficiency (η_{tt}) and total-to-static efficiency (η_{ts}), respectively, as shown in Eqs. (16)-(17).

$$K_N = \frac{P_{01} - P_{02}}{P_{02} - P_2} \tag{14}$$

$$K_R = \frac{P_{02r} - P_{03r}}{P_{03r} - P_3} \tag{15}$$

$$\eta_{tt} = \frac{1}{1 + [K_R W_3^2/2 + (K_N C_2^2/2)(h_3/h_2)]/(h_{01} - h_{03})} \tag{16}$$

$$\eta_{ts} = \frac{1}{1 + [K_R W_3^2/2 + (K_N C_2^2/2)(h_3/h_2) + C_3^2/2]/(h_{01} - h_{03})} \tag{17}$$

Eqs. (16)-(17) indicate that velocity triangles, state quantities, and pressure loss coefficients closely affect turbine efficiency. Meanwhile, Al Jubori et al. (2017a) used a pressure loss model to reach maximum efficiency of radial outflow turbines.

However, the efficiency of the turbine is closely related to the efficiency of the thermodynamic cycle. If the turbine efficiency considered in the thermodynamic cycle and the actual turbine efficiency differ greatly, it is unlikely that the ideal cycle efficiency considered in the thermodynamic cycle will be achieved. In this study, a pressure loss model was used to design a turbine that can achieve the target efficiency. More specifically, after determining the velocity triangle, state 2 corresponding to the nozzle exit in Fig. 10 is an unclear parameter. The nozzle exit point has a great impact on the efficiency of the turbine, as shown in Eqs. (14)-(17) and is an important variable that determines the height of the turbine blades through a continuous equation.

Therefore, in this study, a pressure loss model was used to accurately predict the shape of the blade and the state quantities of the nozzle exit. A flowchart of the preliminary design algorithm presented in this study is shown in Fig. 11. The algorithm was coded using Mathworks MATLAB R2016a and the database of Nist Refprop V9.1 was used to determine the properties and state quantities of the working fluids.

The preliminary design program for a radial outflow turbine developed in this study is based on the following assumptions:

(1) A standard stage is applied, and the tangential absolute velocity component of the rotor exit ($C_{3\theta}$) is zero.

(2) The absolute velocity of the meridian (radius) is constant.

(3) The height of the nozzle blade and the rotor blade is constant.

(4) The velocity ratio (ν) is 0.7.

(5) The deviation angle of the blade is ignored.

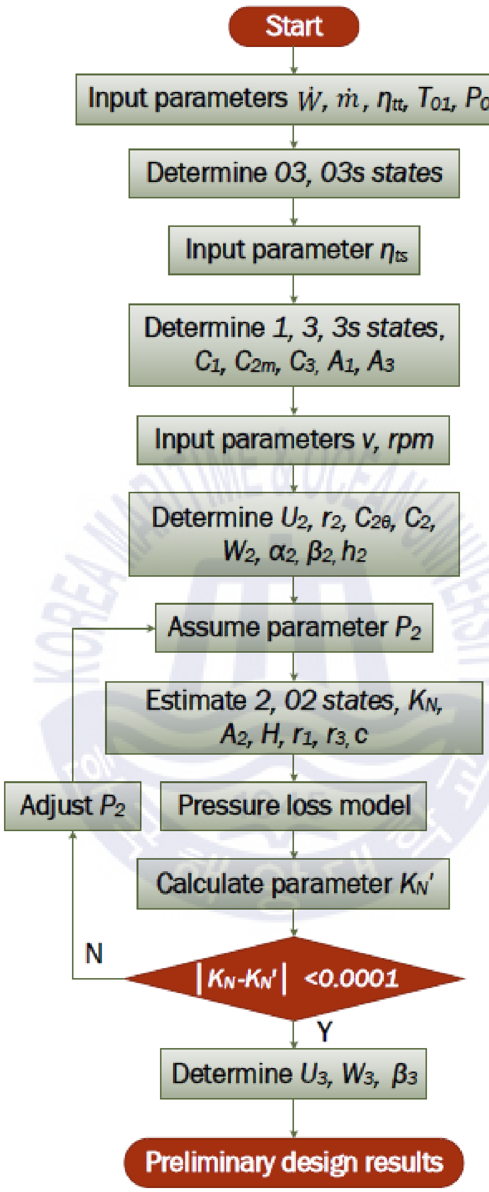

Fig. 11 Flow chart of preliminary design for a radial outflow turbine

The algorithm in Fig. 11 is structured by entering the design conditions of the thermodynamic cycle, target efficiency and rotor rotational speed. Then, the velocity ratio (ν) of assumption (4) is used to determine the radius of the rotor inlet corresponding to the nozzle exit and velocity triangle of the nozzle. In order to determine the shape of the blade and the state quantities of the nozzle exit, the static pressure of the nozzle exit (P_2) is repeatedly calculated by using the pressure loss model. Based on the results and assumptions, the velocity triangle and initial shape of the turbine blade that meet the target efficiency (η_{ts}) are determined.

The pressure loss coefficient, which is a key factor of the algorithm, is given by Eq. (18). I consider profile loss and secondary loss in this study, as they both have a substantial influence on the pressure loss of the blade (Moustapha et al., 2003). In Eq. (18), the first term on the right side represents the profile loss, the second term represents the secondary loss.

$$K_N{}' = f_{Re} K_P + K_{Sec} \tag{18}$$

The K_P of the profile loss is expressed as Eq. (19). Based on the experimental results of Ainley and Mathieson (1951), K_P^* in Eq. (19) is defined as Eq. (20) (Aungier, 2006). According to Moustapha et al. (2003), K_{accel} and K_{sh} in Eq. (19) can be represented by Eqs. (21) and (22), respectively.

$$K_P = 0.914\left(\frac{2}{3} K_P{}^* K_{accel} + K_{sh}\right) \tag{19}$$

$$K_P{}^* = \begin{cases} 0.025 + (27 - \alpha_2{}')/530 & , \alpha_2{}' \leq 27^\circ \\ 0.025 + (27 - \alpha_2{}')/3085 & , \alpha_2{}' > 27^\circ \end{cases} \tag{20}$$

$where,\ \alpha_2{}' = 90 - \alpha_2$

$$K_{accel} = 1 - K_2(1 - K_1) \tag{21}$$

$where,$

$$K_1 = \begin{cases} 1.0 & , M_2 \leq 0.2 \\ 1 - 1.25(M_2 - 0.2) & , M_2 > 0.2 \end{cases}$$

$$K_2 = (M_1 / M_2)^2$$

$$K_{sh} = 0.75(M_1 - 0.4)^{1.75} \left(\frac{P_1}{P_2} \right) \frac{1 - (1 + \frac{k-1}{2} M_1^2)^{k/(k-1)}}{1 - (1 + \frac{k-1}{2} M_2^2)^{k/(k-1)}} \tag{22}$$

Profile loss should be corrected by Reynolds number (Re_{ref}), where f_{Re} in Eq. (18) is the same as Eq. (23).

$$f_{Re} = \begin{cases} (Re_{ref}/2 \times 10^5)^{-0.4} & , Re_{ref} \leq 2 \times 10^5 \\ 1.0 & , 2 \times 10^5 < Re_{ref} \leq 10^6 \\ (Re_{ref}/10^6)^{-0.2} & , Re_{ref} > 10^6 \end{cases} \tag{23}$$

Aungier (2006) suggested the pitch/chord (s/c) as shown Eq. (24) to minimize the pressure drop in the nozzle blade.

$$s/c = \begin{cases} 0.46 + \alpha_2'/77 & , \alpha_2' \leq 30^{\circ} \\ 0.614 + \alpha_2'/130 & , \alpha_2' > 30^{\circ} \end{cases} \tag{24}$$

$where, \alpha_2' = 90 - \alpha_2$

Meanwhile, the second loss coefficient (K_{Sec}) proposed by Moustapha et al. (2003) is given by Eq. (25).

$$K_{Sec} = 0.0334 f_{AS} \left(\frac{\cos\alpha_2}{\cos\alpha_{1b}} \right) \left(\frac{C_L}{s/c} \right)^2 \frac{\cos^2\alpha_2}{\cos^3\alpha_m} \tag{25}$$

$where,$

$$f_{AS} = \begin{cases} \dfrac{1 - 0.25\sqrt{2 - h/c}}{h/c} & , h/c \leq 2 \\ \dfrac{1}{h/c} & , h/c > 2 \end{cases}$$

$$\frac{C_L}{s/c} = 2(\tan\alpha_1 + \tan\alpha_2)\cos\alpha_m$$

$$\alpha_m = \tan^{-1}[0.5(\tan\alpha_1 - \tan\alpha_2)]$$

Chapter 3. Radial outflow turbine for a supercritical CO_2 power cycle

3.1 Design condition

The proposed preliminary design technique for radial outflow turbines should be evaluated through case studies. That is, it should be confirmed that the turbine design is possible according to the design conditions of each case study.

In this chapter, I present a case study on the design of the radial outflow turbine for a supercritical CO_2 power cycle using the preliminary design program developed.

To calculate the main specifications of the turbine, the design conditions of the turbine must be entered into the preliminary design program. The design conditions are detailed in Table 1 with reference to the study of Luo et al. (2017) dealing with the design of a radial outflow turbine for a supercritical CO_2 power cycle. The design conditions required in this program are the power, mass flow rate, turbine inlet pressure and temperature, and RPM. In addition, as mentioned earlier, it is necessary to clearly specify the target efficiency of the turbine. Table 2 shows the properties and information of CO_2 used as a working fluid.

Table 1 Design parameters of preliminary design for a radial outflow turbine

Parameters	Units	Values
Working fluid	-	CO_2
$\dot{W}$	MW	10.0
$\dot{m}$	kg/s	182.46
P_{01}	MPa	13.0
T_{01}	K	773.0
η_{tt}	%	85.0
η_{ts}	%	80.0
RPM	rev/min	6,000

Table 2 Properties and information of CO_2

Parameters	Units	Values
CAS no.	-	124-38-9
Chemical formula	-	CO_2
Molar mass	kg/kmole	44.01
NBP[1)]	K	194.69
Critical temperature	K	304.13
Critical pressure	MPa	7.3773
Critical density	kg/m^3	467.6
Acentric factor	-	0.22394
ALT[2)]	years	>50
ODP[3)]	-	0
GWP[4)]	-	1

1) NBP : Normal Boiling Point
2) ALT : Atmosphere Life Time
3) ODP : Ozone Depletion Potential
4) GWP : Global Warming Potential

3.2 Results of preliminary design

The main specifications of the radial outflow turbine proposed by the preliminary design program are listed in Table 3. These were based on the design conditions in Table 1. In addition, the static pressure in state 2 (P_2) determined by iterative calculation is 10.249 MPa, and the static pressure at the rotor exit (P_3) is 8.001 MPa.

The s/c value of the nozzle determined by Eq. (24) is 0.76, which means that the number of nozzle blades should be 41. When the number of nozzle blades and the number of rotor blades are the same, there is a possibility of resonance occurring, so the number of rotor blades is determined to be 39.

Table 3 Results of preliminary design for the radial outflow turbine

Parameters	Units	Values
r_1	mm	345.393
r_{2N}	mm	408.392
r_{2R}	mm	412.392
r_3	mm	504.560
H	mm	10.843
α_{1b}	°	0
α_{2b}	°	66.87
β_{2b}	°	-27.78
β_{3b}	°	-74.10

3.3 Results of CFD analysis

In this study, CFD was used to verify the preliminary design results of the radial outflow turbine. Using the preliminary design results in Table 3, the single-passage geometry of the radial outflow turbine was constructed as shown in Fig. 12, using ANSYS-BladeGen V13.0. Based on the shape, hexagonal meshes were generated for each nozzle and rotor using ANSYS-TurboGrid V13.0.

ANSYS-CFX V13.0 was used as the CFD analysis program. The equation of state for the working fluid CO_2 uses the Aungier-Redlich-Kwong equation (Eq. (26)), which is reliable even in near critical conditions (Aungier, 2006).

$$P = \frac{RT}{V-b+c} - \frac{a}{V(V+b)T_r^n} \tag{26}$$

$where,$

$$a = 0.42747 R^2 T_c^2 / P_c$$

$$b = 0.08664 R T_c / P_c$$

$$n = 0.4986 + 1.1735\omega + 0.4754\omega^2$$

$$T_r = T / T_c$$

In the above equation, the constant c is directly calculated by applying Eq. (26) at the critical point with all properties specified, and ω means acentric factor (Aungier, 2006).

The turbulence model uses a shear stress transport (SST) model for accurate flow prediction in boundary layers. Considering a single passage, the inlet boundary conditions were set to the mass flow rate (4.45 kg/s = 182.46

kg/s ÷ 41 passages) and the total temperature (773.0 K), as shown in Table 1. The exit boundary condition was set to the static pressure (8.001 MPa) as a preliminary design result. The rotational speed of the rotor domain was 6,000 RPM with the same preliminary design condition. A frozen rotor model was used for the interface between the nozzle and the rotor domain.

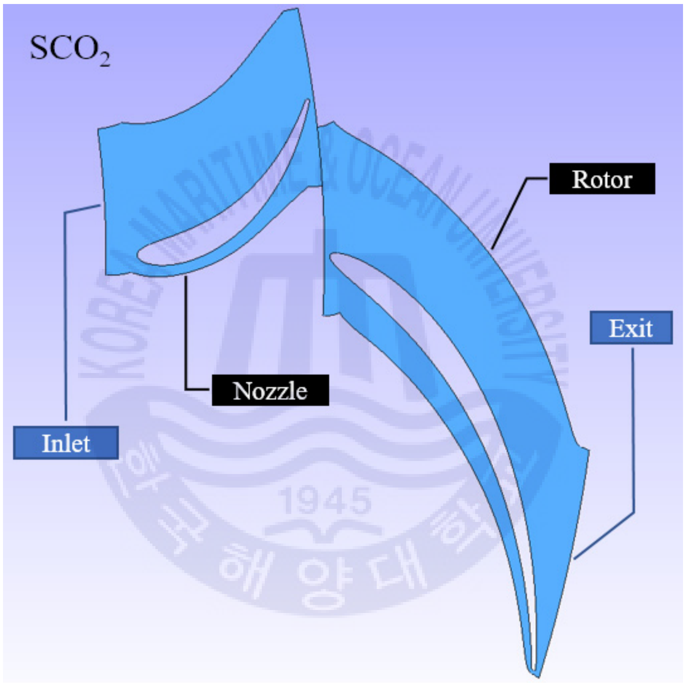

Fig. 12 One-passage geometry of the radial outflow turbine

Table 4 compares the CFD analysis results with the preliminary design conditions and results. Table 4 shows that the preliminary designed radial outflow turbine does not meet the design target power ($\dot{W}$) and efficiency (η_{ts}).

The CFD analysis results show that the values of $C_{2\theta}$ differ because the nozzle blades do not sufficiently accelerate the working fluid. The value of $C_{3\theta}$ is relatively high, and the specific power of the turbine is reduced.

Meanwhile, the preliminary design program of this study ignored the deviation angles of the nozzle and rotor blades as per assumption (5). It was assumed that for the velocity triangle completed in the preliminary design, each exit angle of the nozzle blade (α_{2b}) and rotor blade (β_{3b}) was equal to the absolute velocity angle of the nozzle exit (α_2) and the relative velocity angle of the rotor exit (β_3), respectively. Table 4 shows that this resulted in each deviation angle of the nozzle and rotor differing by approximately 6° and 2°, respectively.

There are few references that point to the importance of deviation angles in research cases of radial outflow turbines. However, the results in Table 4 indicate that the deviation angle should be considered in the design of the radial outflow turbine to satisfy the target performance and velocity triangle at each point.

Table 4 Comparison between results of preliminary design and CFD

Parameters	Preliminary design	CFD
P_{01} [MPa]	13.00	11.08
$\dot{W}$ [MW]	10.00	6.50
η_{ts} [%]	80.00	77.50
α_2 [°]	66.87	60.89
β_3 [°]	-74.10	-72.11
C_2 [m/s]	230.01	205.35
$C_{2\theta}$ [m/s]	211.52	177.52
$C_{3\theta}$ [m/s]	0	32.86

3.4 Optimization of velocity triangles

3.4.1 Optimization procedure

Optimization of the radial outflow turbine was undertaken to satisfy the velocity triangle presented by the preliminary design program. This optimization process is shown in Fig. 13.

The velocity triangles at the inlet and exit of the nozzle located upstream of the rotor are independent of the rotor. That is, the rotor domain is unnecessary in the CFD for determining the optimization of the velocity triangle of the nozzle. Thus, during optimization of the nozzle blade, only the nozzle domain was used, and the rotor domain was excluded. Then, the velocity triangle optimization of the nozzle was performed by adjusting only the exit angle of the nozzle blade (α_{2b}). The optimization results of the nozzle blade were used to adjust the exit angle of the rotor blade (β_{3b}) to optimize the velocity triangle of the rotor.

3.4.2 Optimization of nozzle velocity triangle

The exit angle of the nozzle blade (α_{2b}) was modified giving consideration to the deviation angle. The optimization of the nozzle velocity triangle was confirmed using CFD. Here, the boundary condition of the nozzle exit was 10.249 MPa, which is the static pressure of the nozzle exit (P_2) proposed by the preliminary design program. Other boundary conditions and settings are as described in Section 3.3.

Fig. 14 shows the variation in the total pressure of the nozzle inlet (P_{01}) and the tangential absolute velocity of the nozzle exit ($C_{2\theta}$) according to the change in the exit angle of the nozzle blade (α_{2b}). The total pressure of the nozzle inlet (P_{01}) and the tangential absolute velocity of the nozzle exit ($C_{2\theta}$) as per the preliminary design program are 13.0 MPa and 211.52 m/s, respectively. From Fig. 14, when α_{2b} is 74°, the two variables have appropriate values. The convergence test based on P_{01} when α_{2b} is 74° displayed in Fig. 15. The result, which is not dependent on the number of elements, was obtained at about 3.2 million elements. At this time, P_{01} and $C_{2\theta}$ were 12.80 MPa and 224.36 m/s, respectively.

3.4.3 Optimization of rotor velocity triangle

The velocity triangle of the rotor inlet and outlet is closely related to the nozzle. Therefore, the nozzle blade whose exit angle is adjusted to 74° by the optimization of the nozzle should be included in the CFD analysis for the optimization of the rotor. The boundary condition setting and the CFD analysis method are the same as described in Section 3.3.

The inlet angle of the rotor blade (β_{2b}) was modified to -21.05° by optimizing the nozzle blade. To optimize the rotor blade, the exit angle of the rotor blade (β_{3b}) was adjusted to remove $C_{3\theta}$.

The change in P_{01}, $\dot{W}$, and η_{ts} according to the exit angle of the rotor blade (β_{3b}) is shown in Figs. 16-17. When β_{3b} is -77°, the result is very close to the design condition. The design conditions and CFD analysis results when β_{3b} is -77° are detailed in Table 5.

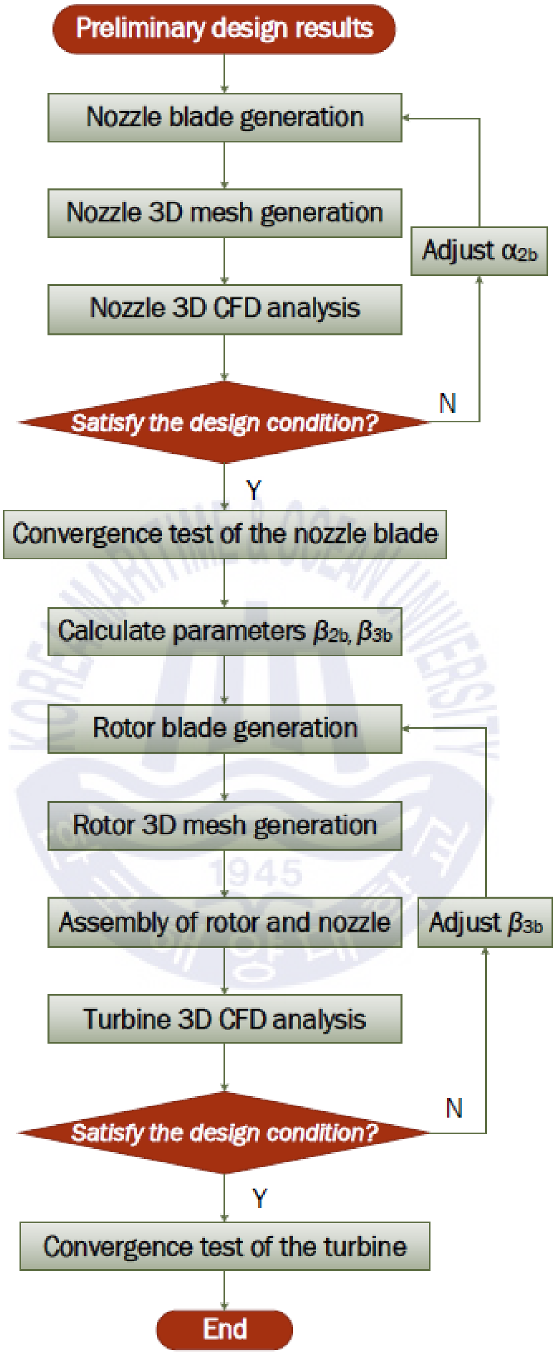

Fig. 13 Flow chart of optimization for the radial outflow turbine

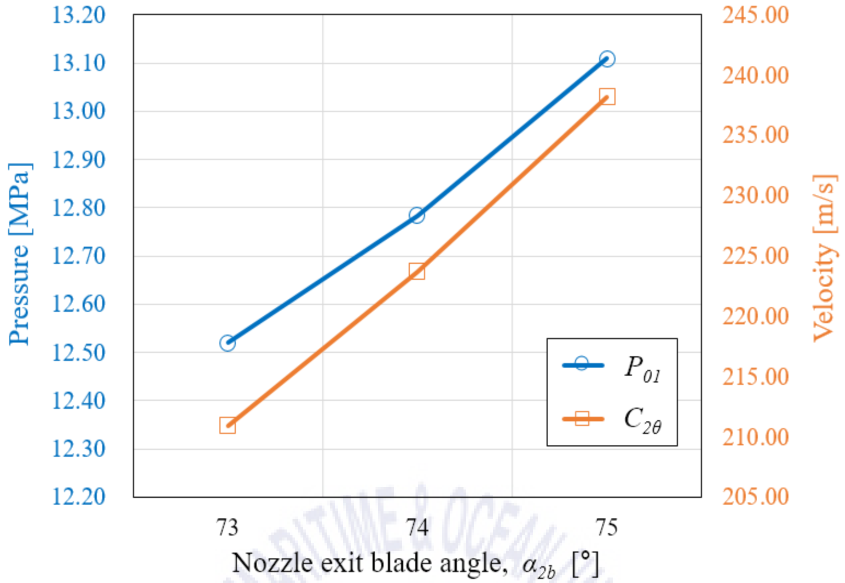

Fig. 14 CFD results according to the nozzle exit blade angle (α_{2b}) of the radial outflow turbine

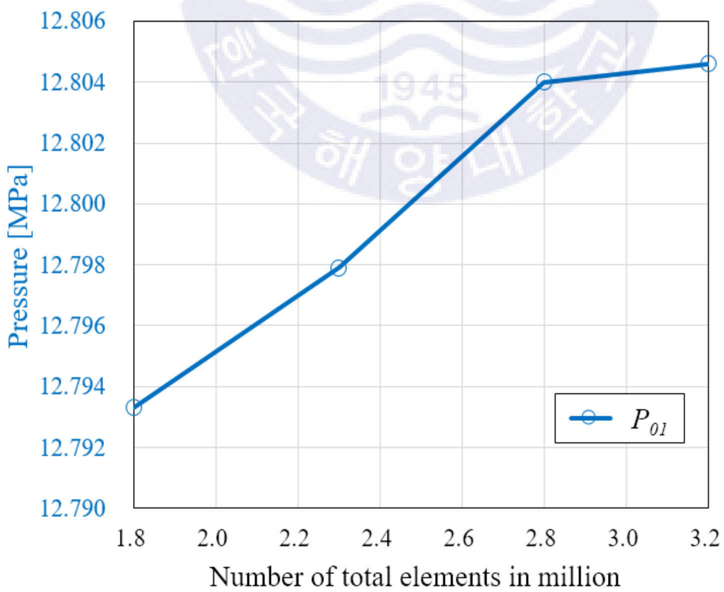

Fig. 15 Convergence test results of the nozzle

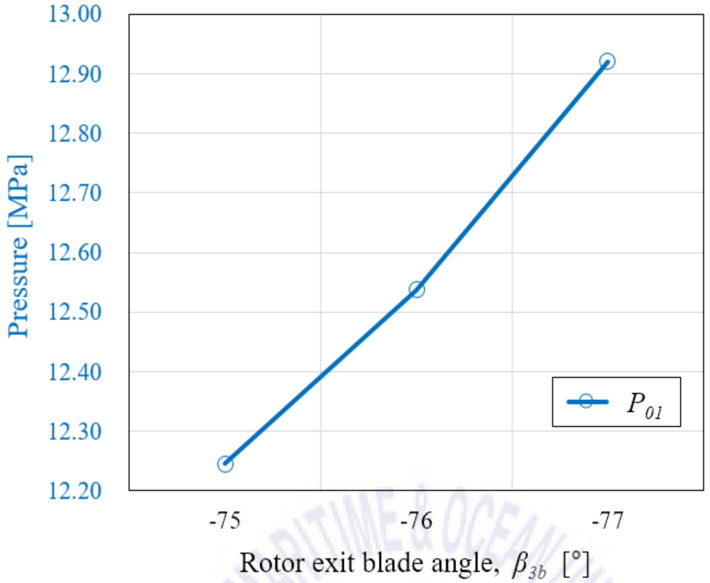

Fig. 16 CFD results according to the rotor exit blade angle (β_{3b}) of the radial outflow turbine (P_{01})

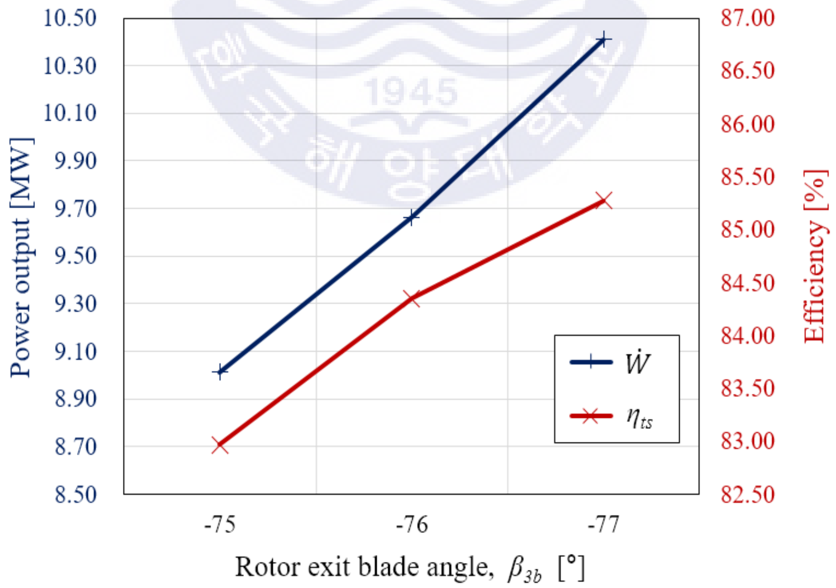

Fig. 17 CFD results according to the rotor exit blade angle (β_{3b}) of the radial outflow turbine ($\dot{W}$ & η_{ts})

Table 5 Comparison between design requirements and CFD results at $\beta_{3b} = -77\,°$

Parameters	Preliminary design	CFD
P_{01} [MPa]	13.00	12.92
$\dot{W}$ [MW]	10.00	10.41
η_{ts} [%]	80.00	85.27

3.5 Performance evaluation of final geometry

3.5.1 Final geometry

The main specifications of the radial outflow turbine for a supercritical CO_2 power cycle finally obtained through the above optimization process are listed in Table 6. Table 6 shows that only the nozzle exit angle and rotor inlet/exit angle were modified through the optimization process.

Table 6 Comparison between results of preliminary design and optimization

Parameters	Preliminary design	Optimization results
r_1 [mm]	345.393	345.393
r_{2N} [mm]	408.392	408.392
r_{2R} [mm]	412.392	412.392
r_3 [mm]	504.560	504.560
H [mm]	10.843	10.843
α_{1b} [°]	0	0
α_{2b} [°]	66.87	74.0
β_{2b} [°]	-27.78	-21.05
β_{3b} [°]	-74.10	-77.0

3.5.2 Convergence test

A convergence test was conducted based on the final shape shown in Table 6. The convergence test results are illustrated in Figs. 18–19. There are about 8.4 million final elements, and detailed information about the grid is presented in Table 7.

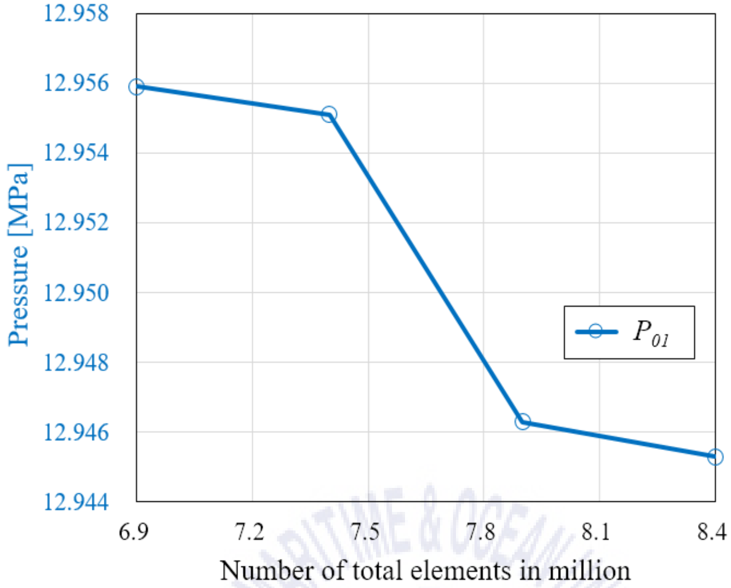

Fig. 18 Convergence test results of the final radial outflow turbine (P_{01})

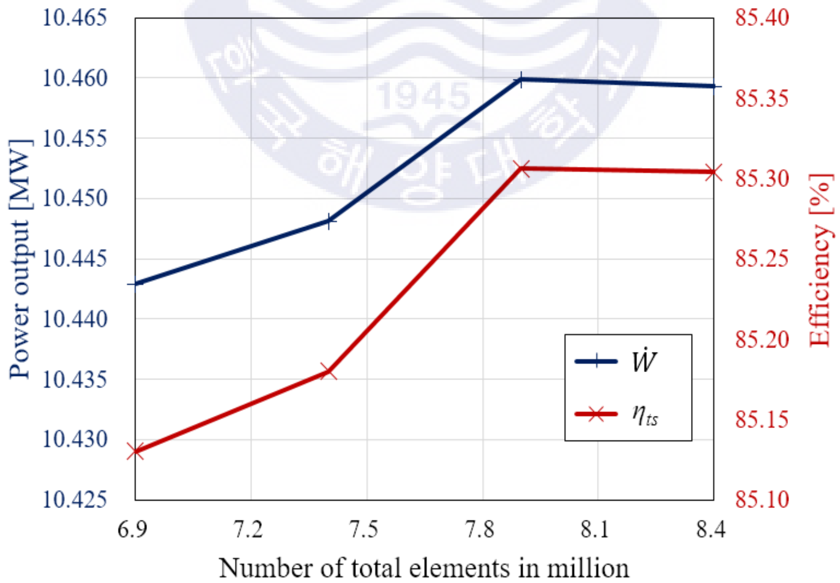

Fig. 19 Convergence test results of the final radial outflow turbine ($\dot{W}$ & η_{ts})

Table 7 Information of final grid

Domain	No. element	max. y+
Nozzle	4,093,581	22.84
Rotor	4,082,892	25.67

3.5.3 Final performance

Table 8 compares the design conditions and performance of the radial outflow turbine designed in this study. The CFD analysis results show that the performance of this radial outflow turbine is in good agreement with the design conditions.

Although the pressure and temperature ratios agree well with the design conditions, the CFD numerical results show that the efficiency of the radial outflow turbine designed in this study exceeds the target design efficiency. This issue is considered intrinsic to ANSYS-CFX.

Sauret and Gu (2014) found that CFX predicts higher turbine efficiency than actual because of the inherent errors in the enthalpy and entropy prediction models used by CFX. More specifically, the inherent errors are caused by the characteristics of the actual gas in which enthalpy and entropy react sensitively to slight temperature differences. In other words, the predicted efficiency of the radial outflow turbine designed in this study exceeds 5.30 % of the design condition, but in practice, this error is expected to be somewhat reduced.

Table 8 Performance of the radial outflow turbine

Parameters	Design values	CFD results
PR_{ts} [-]	1.62	1.62
TR_{ts} [-]	1.08	1.07
$\dot{W}$ [MW]	10.00	10.46
η_{ts} [%]	80.00	85.30

3.6 Performance analysis of off-design conditions

In order to understand the off-design performance and to define performance charts of the radial outflow turbine for a supercritical CO_2 power cycle, off-design performance analysis was conducted according to various independent variables. The independent variables considered were the turbine inlet temperature, mass flow rate, and pressure ratio. The change in the rotational speed of the turbine was considered concurrently with each independent variable.

Fig. 20 shows the power output and total-to-static efficiency according to the turbine inlet temperature and rotational speed. The results showed that the power output increases in proportion to the inlet temperature of the turbine at each rotational speed. At the design RPM, turbine efficiency remained highest with changes in turbine inlet temperature. At other RPMs, the turbine efficiency changes rapidly with variations of the turbine inlet temperature.

Fig. 21 shows the power output and total-to-static efficiency according to the mass flow rate and rotational speed. Here, M corresponding to the independent variable, is defined as the mass flow rate of the off-design condition over the mass flow rate of the design condition, as per Eq. (27).

$$M = \frac{mass\,flowrate}{mass\,flowrate_{design}} \tag{27}$$

The power output increases in proportion to the mass flow rate entering the turbine at each rotational speed. At the design RPM, the turbine efficiency continues to rise over the M range of 0.90–1.05 and decreases at

1.10. At other RPMs, the turbine efficiency varies largely with changes to the mass flow rate.

Fig. 22 shows the power output and total-to-static efficiency according to the pressure ratio and rotational speed. The power output increases in proportion to the pressure ratio at each rotational speed. Here, similar outputs are shown at the same pressure ratio regardless of rotational speed. At the design RPM, the turbine efficiency continues to increase to a pressure ratio range of 1.62 and then decreases. At other RPMs, the turbine efficiency varies greatly according to changes in the pressure ratio.

Based on the off-design performance analysis of the radial outflow turbine for the supercritical CO_2 power cycle, the power output increased in proportion to the turbine inlet temperature, mass flow rate, and pressure ratio. Meanwhile, there are features that are common to each of the off-design conditions in turbine efficiency. Typically, when the rotational speed was lower than the design RPM, the turbine efficiency tended to decrease as each independent variable increased. Conversely, when the rotational speed was higher than the design RPM, the turbine efficiency tended to increase with an increase to each independent variable. The design RPM maintained a high range with relatively little change in turbine efficiency based on the change to each independent variable. At other RPMs, the turbine efficiency changes rapidly with changes to each independent variable. These results suggest that operating the turbine to approach the design RPM is advantageous for turbine efficiency.

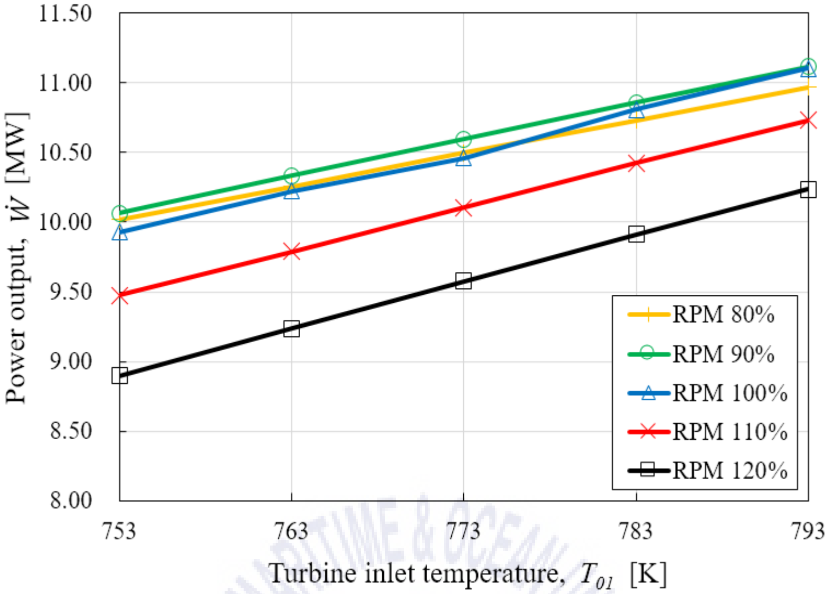

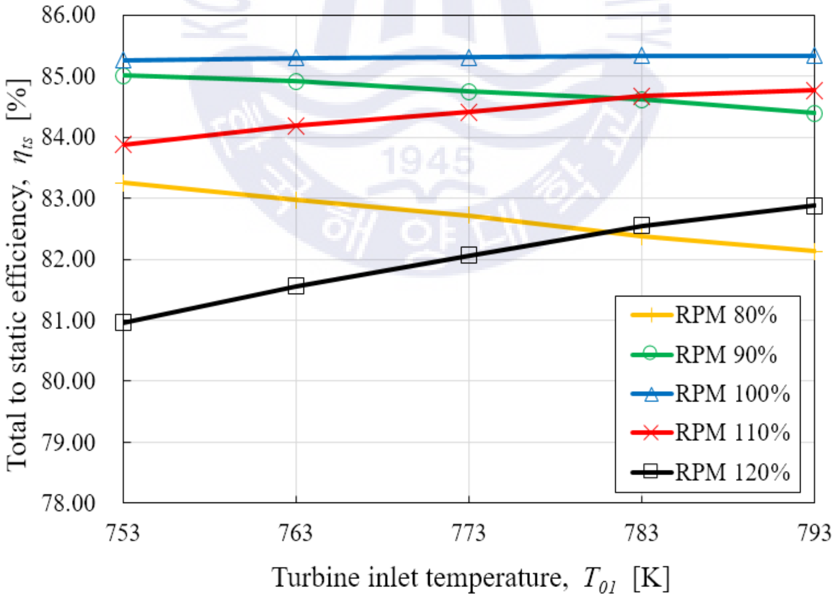

Fig. 20 Power output & total to static efficiency of the radial outflow turbine (T_{01} & RPM)

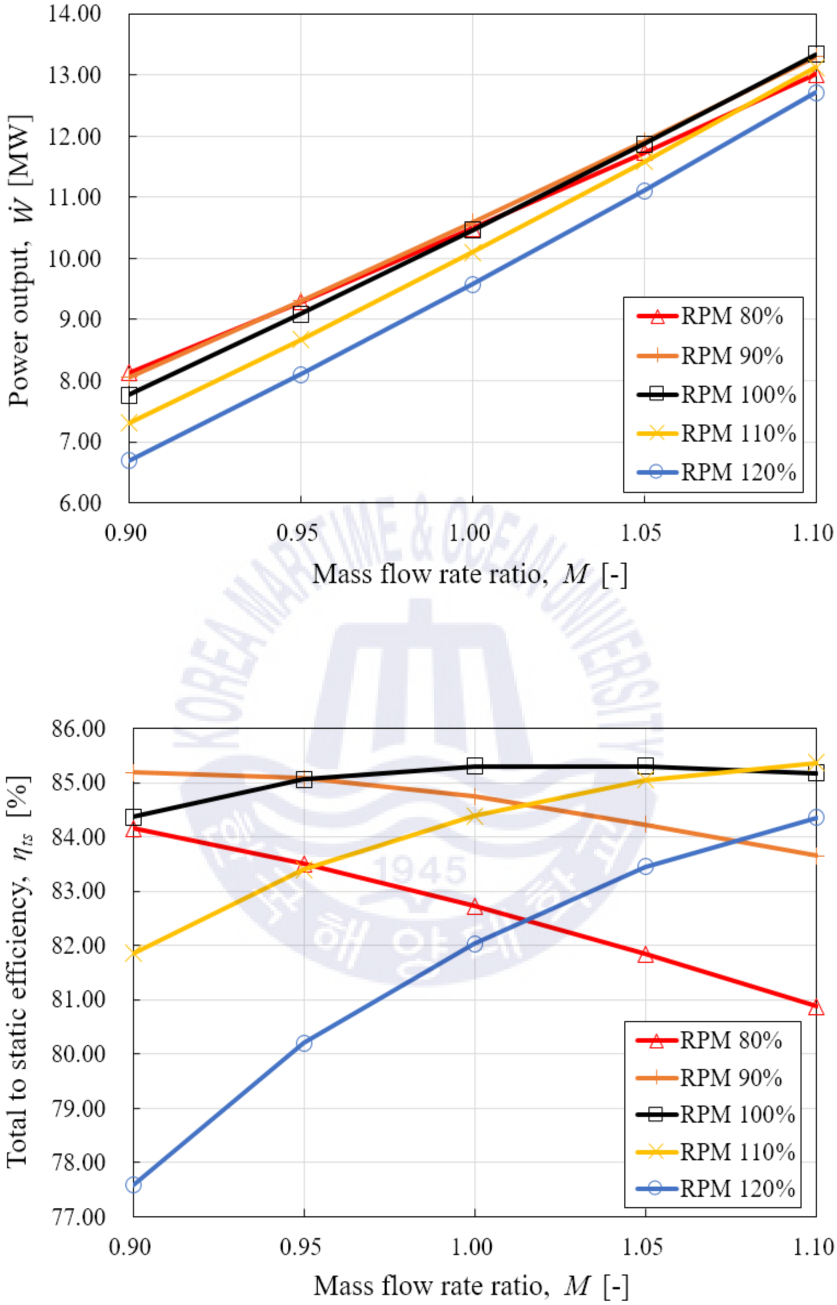

Fig. 21 Power output & total to static efficiency of the radial outflow turbine (M & RPM)

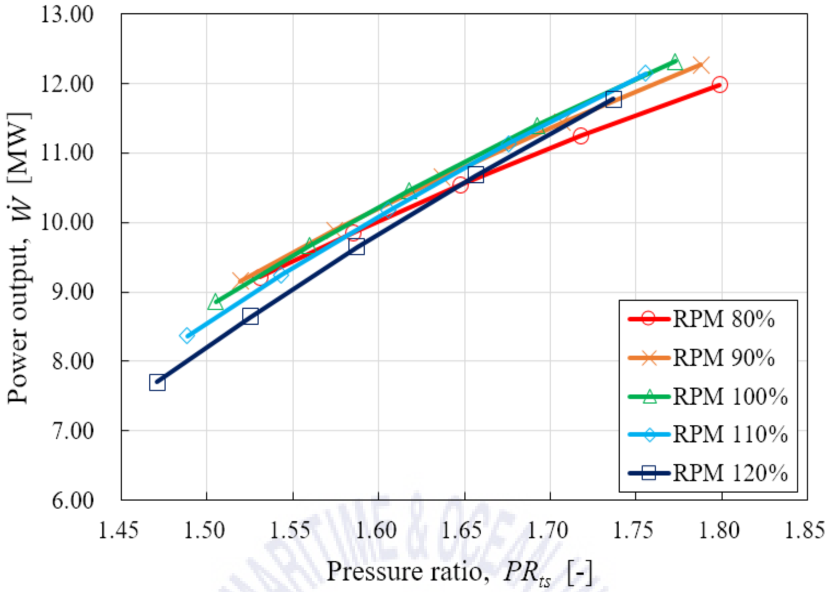

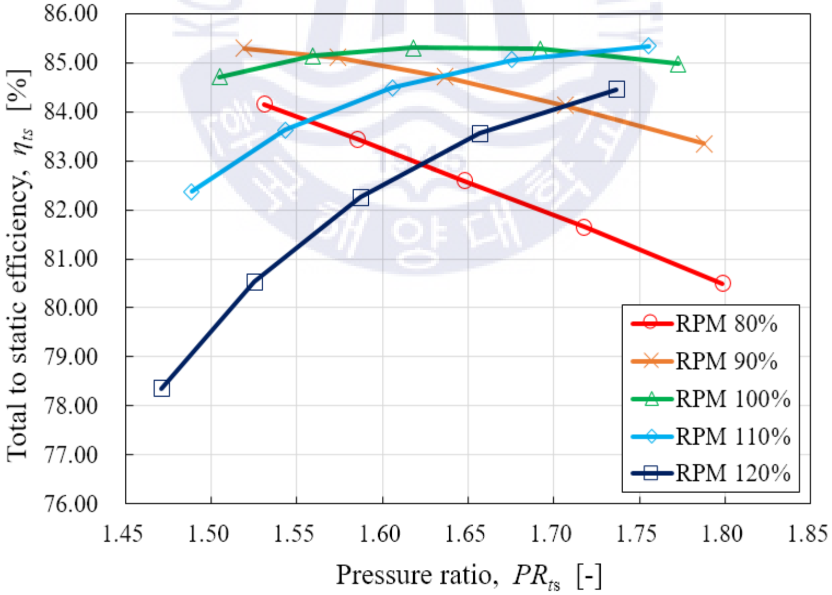

Fig. 22 Power output & total to static efficiency of the radial outflow turbine (PR_{ts} & RPM)

3.7 Performance curve based on dimensionless variables

3.7.1 Performance curve

Using the off-design performance results, Figs. 23–25 present the performance curves of the radial outflow turbine for the supercritical CO_2 power cycle according to the specific speed (N_s), loading coefficient (ψ), and flow coefficient (ϕ).

The performance curves of the turbine show a specific range of dimensionless variables that represent high efficiency. Therefore, if the value of each dimensionless variable is too high or too low, then high efficiency of the turbine is unlikely. The lowest point of turbine efficiency was approximately 77.58 % at the highest specific speed and the lowest loading and flow coefficients.

Table 9 shows the range of dimensionless variables that are likely to have a high efficiency of approximately 85.0 % or more in the turbine's performance curve. In the design of radial outflow turbines for supercritical CO_2 power cycles requiring high efficiency, the range of each dimensionless parameter given in Table 9 can be an important criterion in the determination of key design parameters.

In this study, the CFD numerical analysis results were used to analyze the factors that influence the efficiency of the radial outflow turbine for a supercritical CO_2 power cycle. In Figs. 23–25, each of A, B, and C is the same. Point A corresponds to the design point of the turbine and is in the high-efficiency range. Points B and C are located at both ends of each performance curve and are in a relatively low efficiency range. Point C is the point of lowest efficiency in the performance curve.

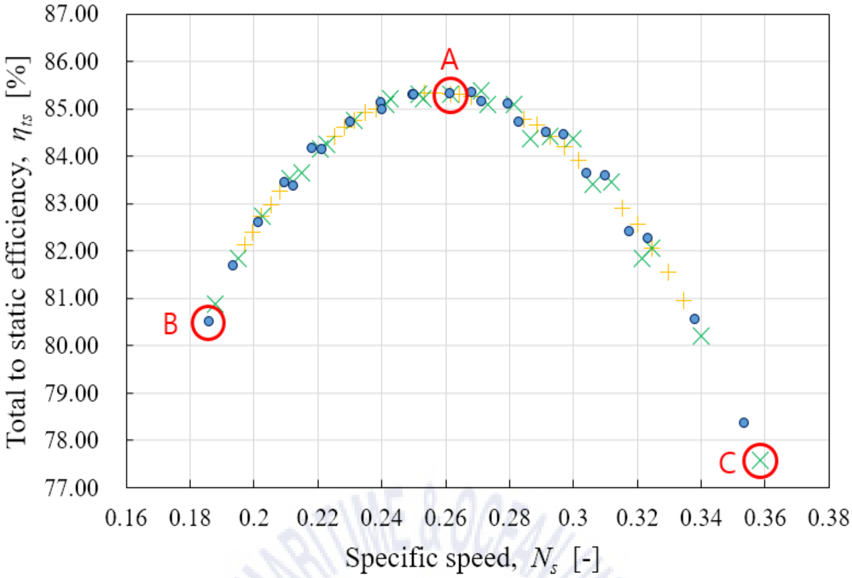

Fig. 23 Performance curve of the radial outflow turbine (N_s)

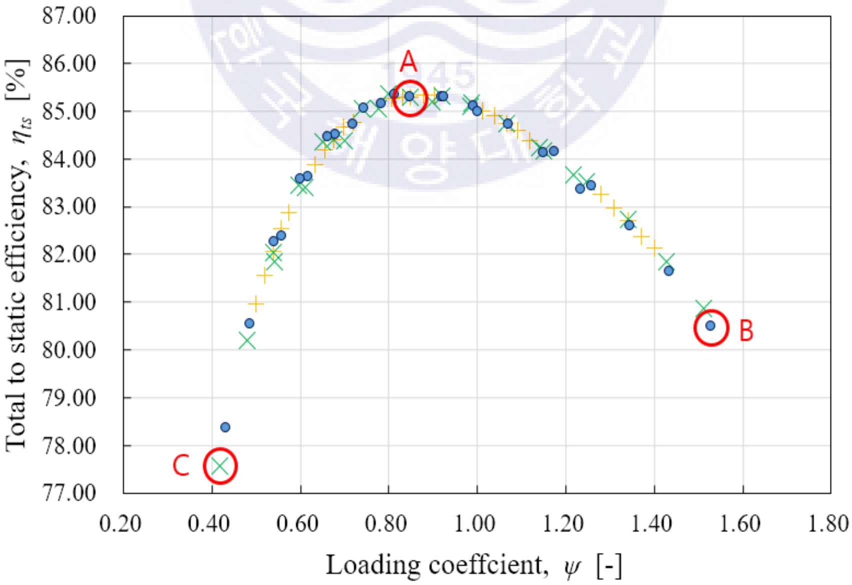

Fig. 24 Performance curve of the radial outflow turbine (ψ)

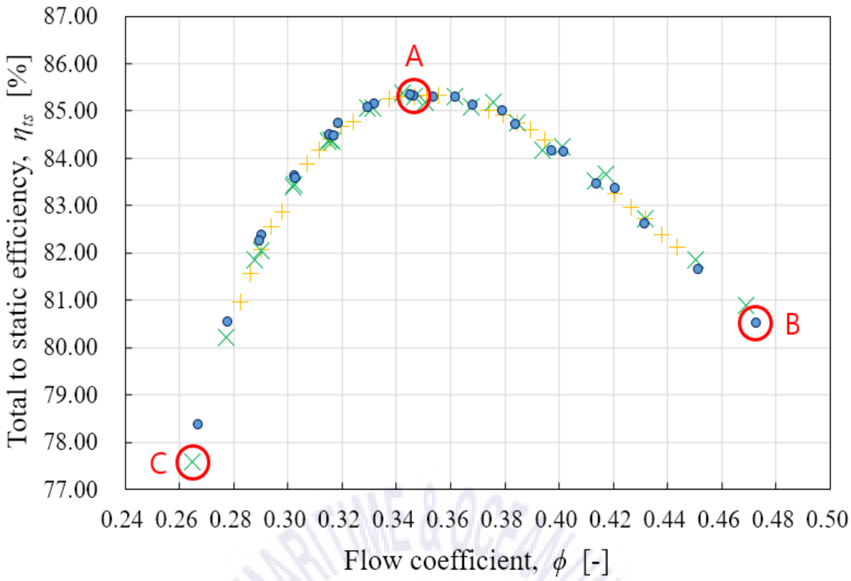

Fig. 25 Performance curve of the radial outflow turbine (ϕ)

Table 9 Range of dimensionless variables for high performance of the radial outflow turbine

Parameters	Range
Specific speed (N_s)	0.24 – 0.28
Loading coefficient (ψ)	0.70 – 1.00
Flow coefficient (ϕ)	0.33 – 0.38

3.7.2 Analysis of CFD results

Fig. 26 shows the static pressure contours for the three passages at points A, B, and C. Looking at points A and B, the pressure decreases appropriately from the inlet of the nozzle blade to the exit of the rotor blade. In addition, the pressure side is always higher than the suction side in all areas of the rotor blades. At point C, there is a region in the rotor blade where the suction side has higher pressure than the pressure side. As the designed rotor rotates counterclockwise, the rotation of the turbine is impeded if the suction side has higher pressure than the pressure side of the rotor blades. This may cause the lowest efficiency in the turbine' s performance curve. Meanwhile, based on the inlet pressure of the nozzle blade, the pressure at point C is lower than that of A and B. Additionally, the pressure ratios of A, B, and C calculated by CFD are 1.62, 1.80, and 1.46, respectively.

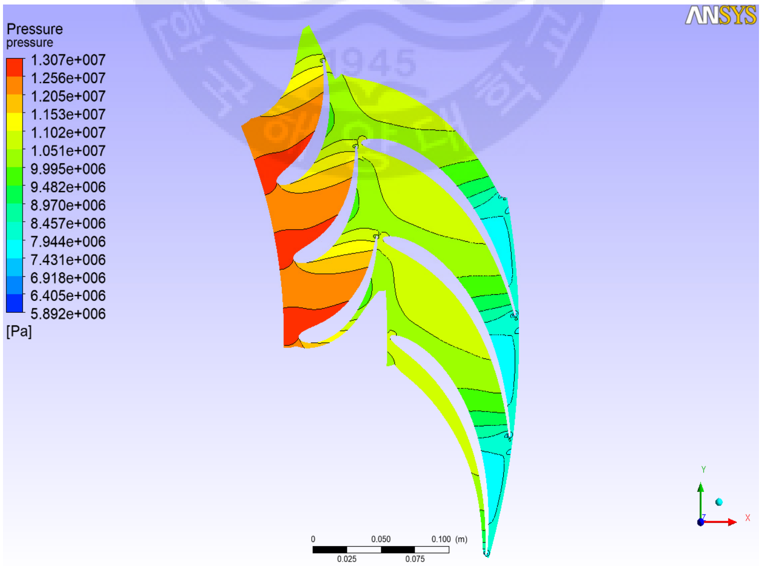

(A)

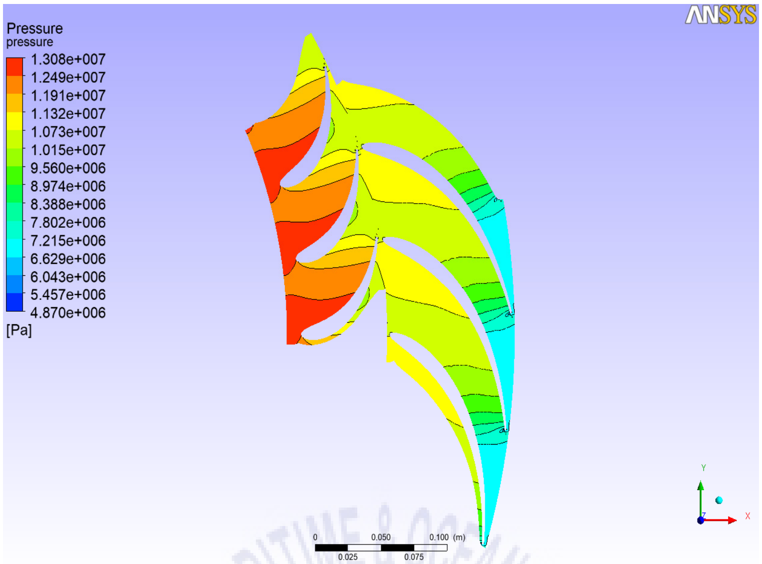

(B)

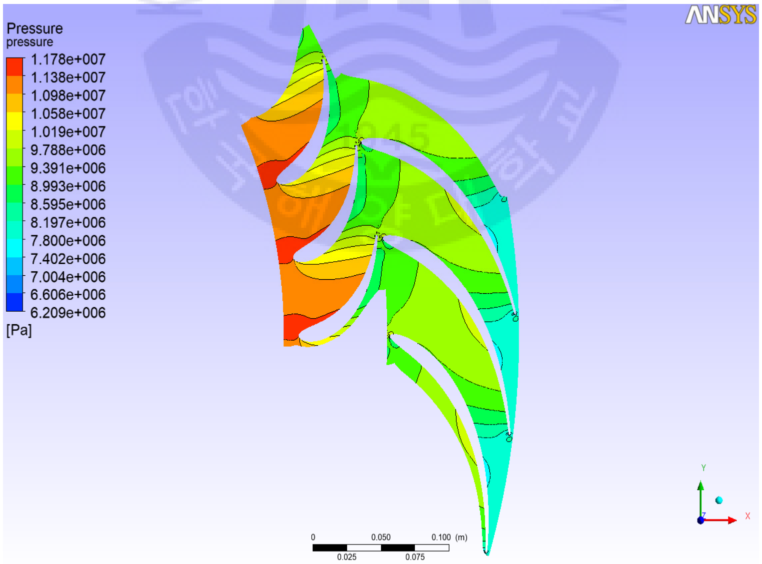

(C)

Fig. 26 Pressure contour of the radial outflow turbine

Fig. 27 shows the velocity contour at each point. The velocity of the nozzle blade represents the absolute velocity, and the velocity of the rotor blade represents the relative velocity. As the fluid in the turbine expands from the inlet to the exit, the absolute velocity increases at the nozzle blades and the relative velocity increases at the rotor blades. In term of the velocity contour, consideration should be given to the position of the stagnation point formed in the rotor blade inlet. At point A, a small stagnation point is formed at the start of the leading edge of the rotor blade, and an appropriate velocity distribution is shown. At point B, the stagnation point is formed relatively wide on a certain pressure side on the leading edge of the rotor blade. At point C, a very small stagnation point appears on the suction side of the leading edge of the rotor blade. When a stagnation point is formed toward the pressure or suction side at the leading edge of the rotor blade, it may affect the reduction in turbine efficiency.

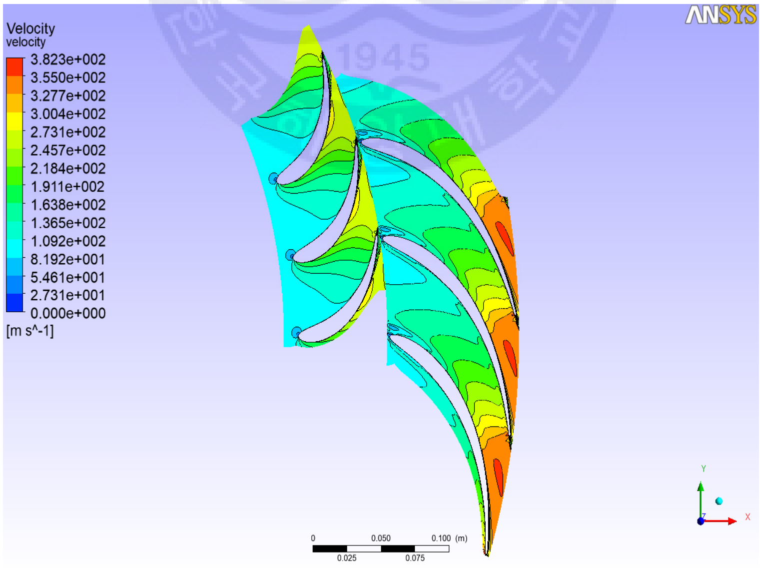

(A)

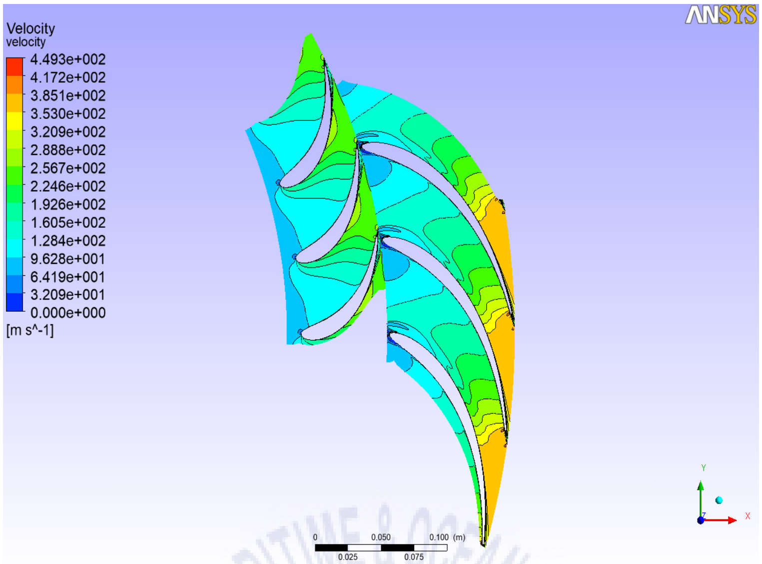

(B)

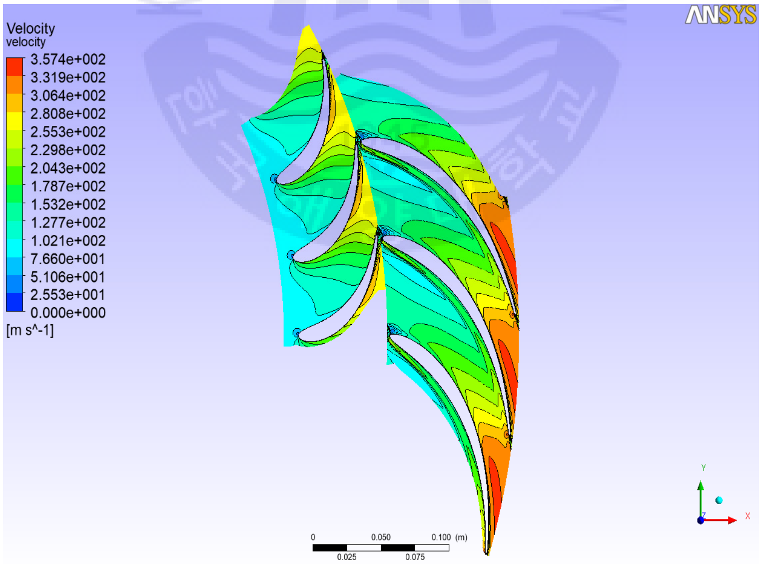

(C)

Fig. 27 Velocity contour of the radial outflow turbine

Fig. 28 illustrates the streamline at each point, which differs at the leading edges of the rotor blades. In terms of the most efficient, point A, a streamline is formed smoothly according to the shape of the rotor blade. At point B, the streamline is directed toward the pressure side at approximately 20.33° from the angle of the rotor blades (β_{2b}). At point C, the streamline is directed toward the suction side at approximately -19.63° from the angle of the rotor blades (β_{2b}). Looking at the difference between the angle of the rotor blade (β_{2b}) and the flow angle (β_2), the angle difference is similar at point B and C. Nevertheless, point C occurs at the lowest point in the turbine's performance curve. This demonstrates that when flow is excessively directed to the suction side rather than the pressure side of the rotor blade, it causes drastic reduction in turbine efficiency.

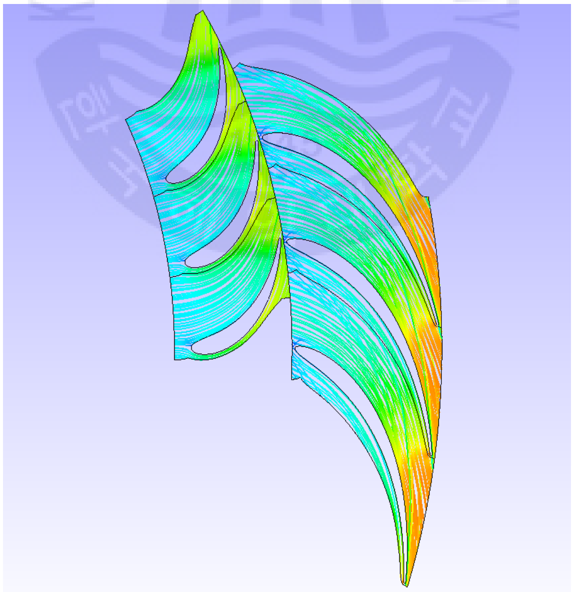

(A)

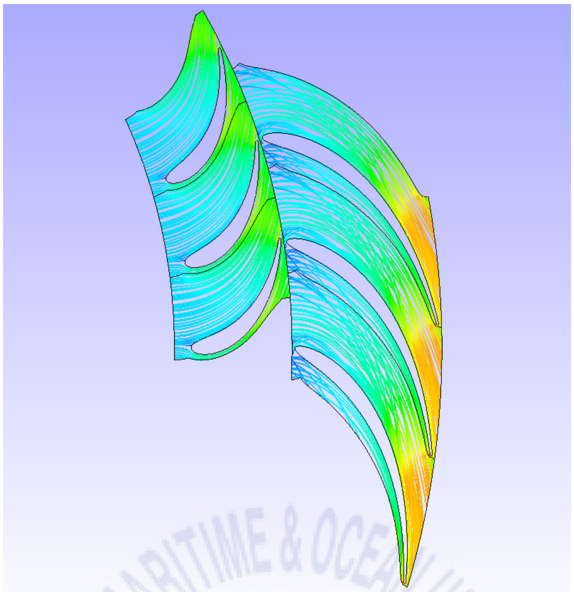

(B)

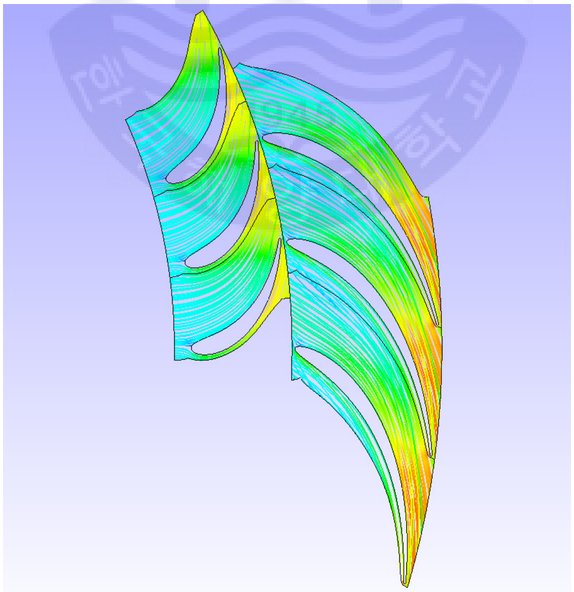

(C)

Fig. 28 Streamline of the radial outflow turbine

Chapter 4. Radial outflow turbine for an organic Rankine cycle

4.1 Design condition

In this chapter, I present a case study on the design of the radial outflow turbine for an organic Rankine cycle using the preliminary design program developed.

In order to obtain the main specifications of the turbine, the design condition of the turbine referred to the study of Sauret and Gu (2014) using working fluid R143a. The study dealt with the design of a radial inflow turbine. As specific speed of the maximum efficiency depends on the turbomachinery, it is necessary to determine the proper revolutions of the radial outflow turbine under the design conditions. Moreover, to prevent a shockwave due to supersonic speed, the Mach number of all fluid flow fields in the turbine was within 0.8, and the point that satisfies the target efficiency was sought. These conditions were satisfied at a rotational speed of 4,100 RPM, and the design conditions of the radial outflow turbine for the organic Rankine cycle are listed in Table 10. Table 11 shows the properties and information of R143a used as a working fluid.

Table 10 Design parameters of preliminary design for a radial outflow turbine

Parameters	Units	Values
Working fluid	-	R143a
$\dot{W}$	kW	400.0
$\dot{m}$	kg/s	44.04
P_{01}	MPa	5.0
T_{01}	K	413.0
η_{tt}	%	85.0
η_{ts}	%	80.0
RPM	rev/min	4,100

Table 11 Properties and information of R143a

Parameters	Units	Values
CAS no.	-	420-46-2
Chemical formula	-	R143a
Molar mass	kg/kmole	84.041
NBP	K	225.91
Critical temperature	K	345.86
Critical pressure	MPa	3.761
Critical density	kg/m^3	431.0
Acentric factor	-	0.2615
ALT	years	52
ODP	-	0
GWP	-	4,800

4.2 Results of preliminary design

Based on the design conditions in Table 10, the main specifications of the radial outflow turbine proposed by the preliminary design program are listed in Table 12. In addition, the static pressure in state 2 (P_2) determined by iterative calculation is 4.085 MPa, and the static pressure at the rotor exit (P_3) is 3.4 MPa.

The s/c value of the nozzle is calculated to be approximately 0.76, with 40 nozzle blades that meet this value. To avoid damage to the turbine due to resonance, the number of rotor blades is determined to be 37.

Table 12 Results of preliminary design for the radial outflow turbine

Parameters	Units	Values
r_1	mm	202.824
r_{2N}	mm	241.676
r_{2R}	mm	245.676
r_3	mm	296.977
H	mm	5.647
α_{1b}	°	0
α_{2b}	°	66.93
β_{2b}	°	-27.85
β_{3b}	°	-73.95

4.3 Results of CFD analysis

As per the previous case study, CFD was used to verify the preliminary design results of a radial outflow turbine for the organic Rankine cycle. From the preliminary design results in Table 12, the single-passage geometry of the radial outflow turbine was constructed as shown in Fig. 29. Based on the shape, hexagonal meshes were generated for each nozzle and rotor.

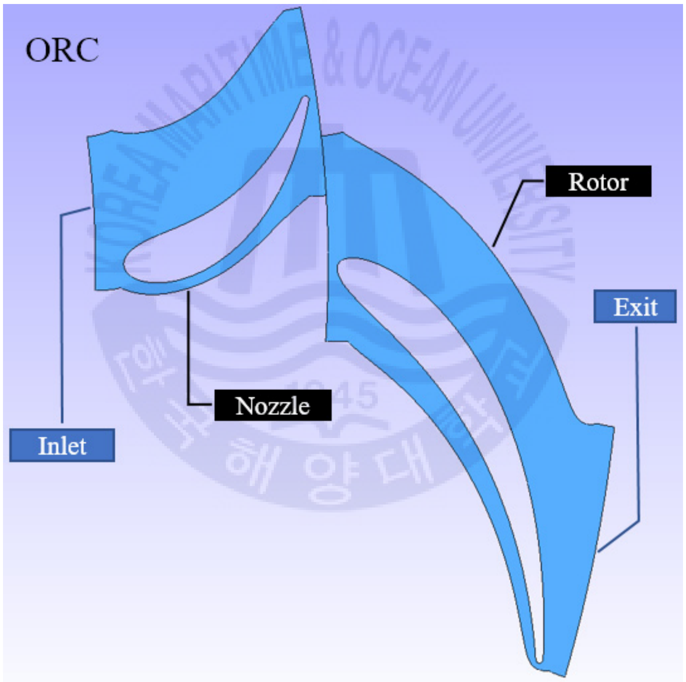

Fig. 29 One-passage geometry of the radial outflow turbine

CFD analysis techniques such as the equation of state and turbulence model were the same as those described in Section 3.3. Considering a single passage, the inlet boundary conditions were set to the mass flow rate (1.10 kg/s =

44.04 kg/s ÷ 40 passages) and the total temperature (413.0 K), as shown in Table 10. The exit boundary condition was set to the static pressure (3.4 MPa) as a preliminary design result. The rotational speed of the rotor domain was 4,100 RPM with the same preliminary design condition.

Table 13 compares the CFD analysis results with the preliminary design conditions and results. It shows that the preliminary designed radial outflow turbine does not meet the design target power ($\dot{W}$) and efficiency (η_{ts}).

The CFD analysis results show that the values of $C_{2\theta}$ and $C_{3\theta}$ differ somewhat from the preliminary design results. This is similar to the results of the previous case study.

This case study also assumed that for the velocity triangle completed in the preliminary design, each exit angle of the nozzle blade (α_{2b}) and rotor blade (β_{3b}) was equal to the absolute velocity angle of the nozzle exit (α_2) and the relative velocity angle of the rotor exit (β_3), respectively. Table 13 shows that this resulted in each deviation angle of the nozzle and rotor differing by approximately 3.2° and 0.3°, respectively.

These results indicate that even in the design of radial outflow turbines for organic Rankine cycles, an optimization process is required to meet the target performance and velocity triangles at each point.

Table 13 Comparison between results of preliminary design and CFD

Parameters	Preliminary design	CFD
P_{01} [MPa]	5.00	4.67
$\dot{W}$ [kW]	400.0	333.38
η_{ts} [%]	80.0	78.05
α_2 [°]	66.93	63.72
β_3 [°]	-73.95	-73.66
C_2 [m/s]	93.59	88.04
$C_{2\theta}$ [m/s]	86.11	78.40
$C_{3\theta}$ [m/s]	0	5.41

4.4 Optimization of velocity triangles

4.4.1 Optimization procedure

Optimization of the radial outflow turbine was performed to satisfy the velocity triangle from the preliminary design program. The optimization of the nozzle and rotor blades was performed sequentially, as per the previous case study. The velocity triangle optimization of the nozzle was performed by adjusting only the exit angle of the nozzle blade (α_{2b}). Based on the optimization result of the nozzle blade, the exit angle of the rotor blade (β_{3b}) was adjusted to optimize the velocity triangle of the rotor.

4.4.2 Optimization of nozzle velocity triangle

The exit angle of the nozzle blade (α_{2b}) was modified giving consideration to the deviation angle, and the optimization of the nozzle velocity triangle was confirmed using CFD. The boundary condition of the nozzle exit was 4.085 MPa, which is the static pressure of the nozzle exit (P_2) proposed by the preliminary design program. Other boundary conditions and settings are as described in Section 4.3.

Fig. 30 shows the variation in the total pressure of the nozzle inlet (P_{01}) and the tangential absolute velocity of the nozzle exit ($C_{2\theta}$) according to the change in the exit angle of the nozzle blade (α_{2b}). The total pressure of the nozzle inlet (P_{01}) and the tangential absolute velocity of the nozzle exit ($C_{2\theta}$) as per the preliminary design program were 5.0 MPa and 86.11 m/s, respectively. Fig. 30 depicts that when α_{2b} is 71°, the two variables have appropriate values. The convergence test based on P_{01} when α_{2b} is 71° is shown in Fig. 31. The result, which is not dependent on the number of elements, was obtained at about 2.5 million elements. At this time, P_{01} and $C_{2\theta}$ were 4.88 MPa and 90.15 m/s, respectively.

4.4.3 Optimization of rotor velocity triangle

The nozzle blade whose exit angle was adjusted to 71° by the optimization of the nozzle should be included in the CFD analysis for the optimization of the rotor. The boundary condition setting and the CFD analysis method are the same as described in Section 4.3.

The inlet angle of the rotor blade (β_{2b}) was modified to -22.01° by optimizing the nozzle blade. To optimize the rotor blade, the exit angle of the rotor blade (β_{3b}) was adjusted to remove $C_{3\theta}$.

The previous case study demonstrated that turbine efficiency decreased significantly when the fluid flow was excessively directed to the suction side at the leading edge of the rotor blade. Therefore, to prevent the inlet flow of the rotor from being directed to the suction side of the rotor blades, the incidence angle was also considered during optimization.

The change in P_{01}, the incidence angle, $\dot{W}$, and η_{ts} according to the exit angle of the rotor blade (β_{3b}) is shown in Figs. 32-33. When β_{3b} is -75°, the result is very close to the design condition, and the inlet flow of the rotor blade is directed toward the pressure side. If β_{3b} is -75°, then the design conditions and CFD analysis results are as listed in Table 14. At this time, the incidence angle of the rotor blade was about 1.86°. A positive value of the incidence angle means that the inlet flow of the rotor blades is directed toward the pressure side.

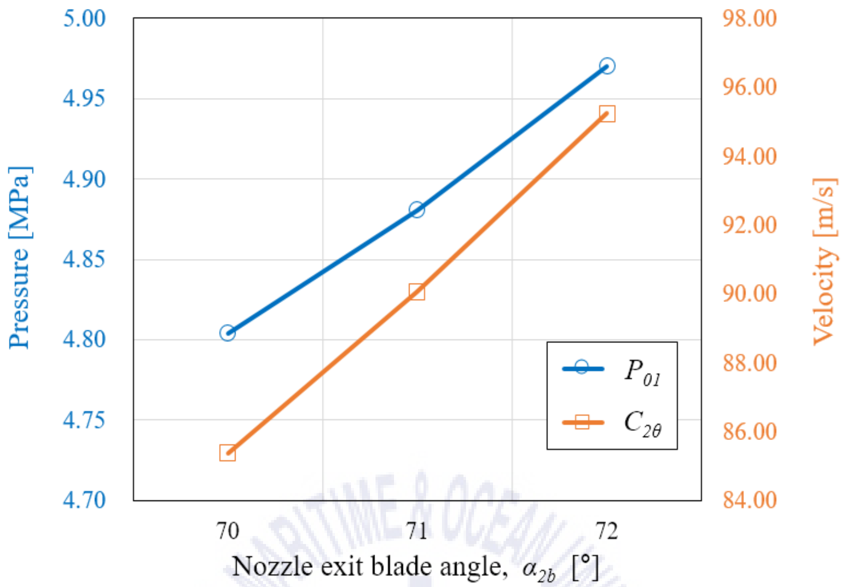

Fig. 30 CFD results according to the nozzle exit blade angle (α_{2b}) of the radial outflow turbine

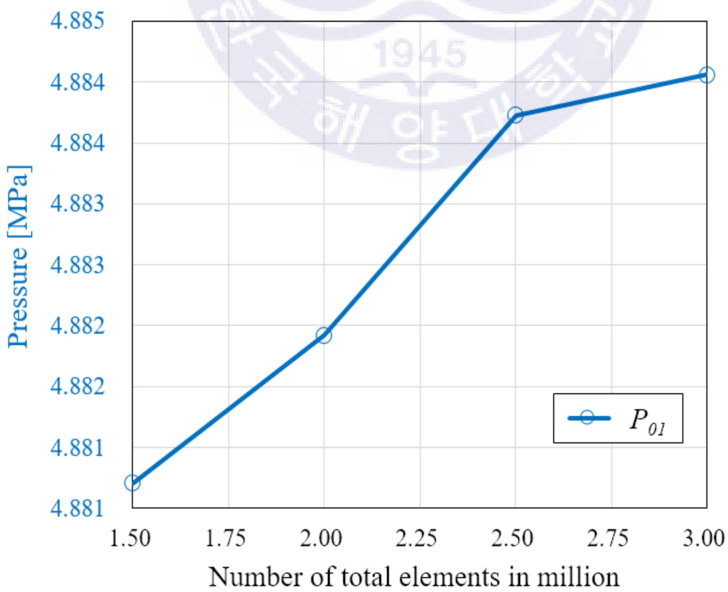

Fig. 31 Convergence test results of the nozzle

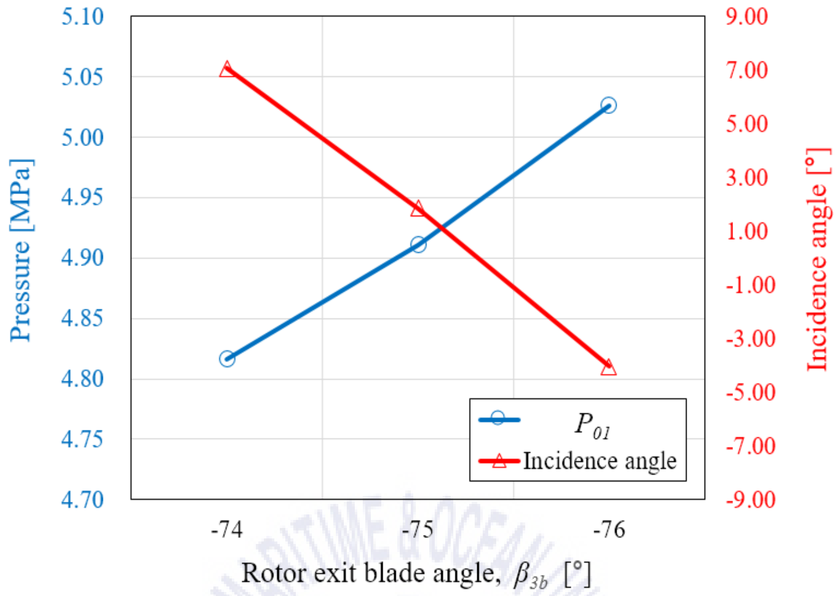

Fig. 32 CFD results according to the rotor exit blade angle (β_{3b}) of the radial outflow turbine (P_{01} & Incidence angle)

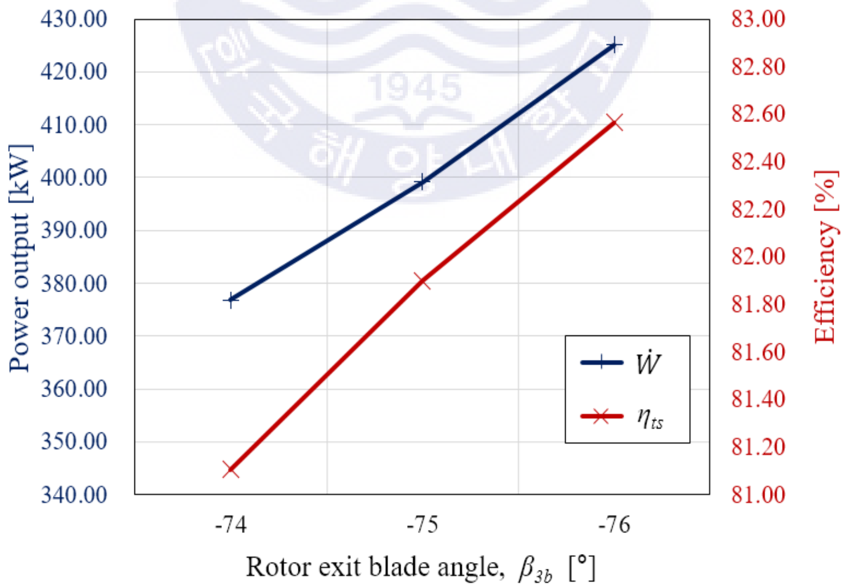

Fig. 33 CFD results according to the rotor exit blade angle (β_{3b}) of the radial outflow turbine ($\dot{W}$ & η_{ts})

Table 14 Comparison between design requirements and CFD results at $\beta_{3b} = -75^{\circ}$

Parameters	Preliminary design	CFD
P_{01} [MPa]	5.00	4.91
$\dot{W}$ [kW]	400.00	399.21
η_{ts} [%]	80.00	81.90

4.5 Performance evaluation of final geometry

4.5.1 Final geometry

Table 15 lists the main specifications of the radial outflow turbine for an organic Rankine cycle obtained through the above optimization process. It shows that only the nozzle exit angle and rotor inlet/exit angle were modified during optimization.

Table 15 Comparison between results of preliminary design and optimization

Parameters	Preliminary design	Optimization results
r_1 [mm]	202.824	202.824
r_{2N} [mm]	241.676	241.676
r_{2R} [mm]	245.676	245.676
r_3 [mm]	296.977	296.977
H [mm]	5.647	5.647
α_{1b} [°]	0	0
α_{2b} [°]	66.93	71.00
β_{2b} [°]	-27.85	-22.01
β_{3b} [°]	-73.95	-75.00

4.5.2 Convergence test

A convergence test was conducted based on the final shape shown in Table 15. The convergence test results are shown in Figs. 34–35. There are approximately 9 million final elements, Table 16 provides detailed information about the grid.

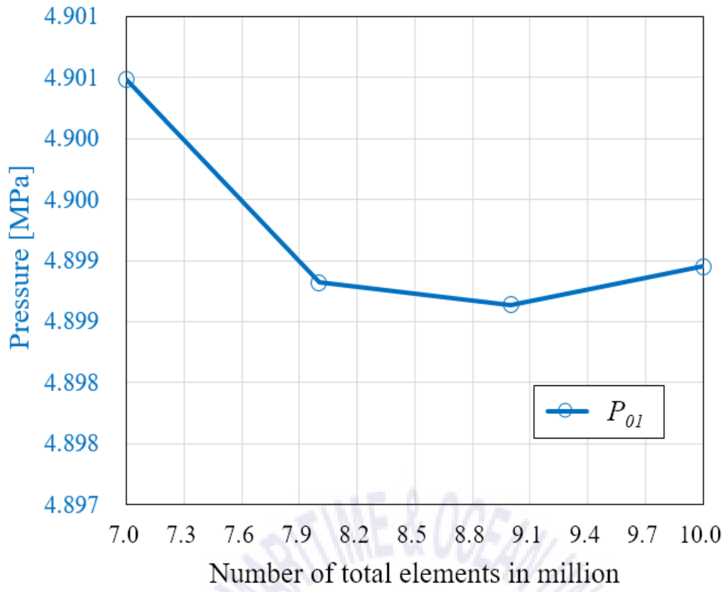

Fig. 34 Convergence test results of the final radial outflow turbine (P_{01})

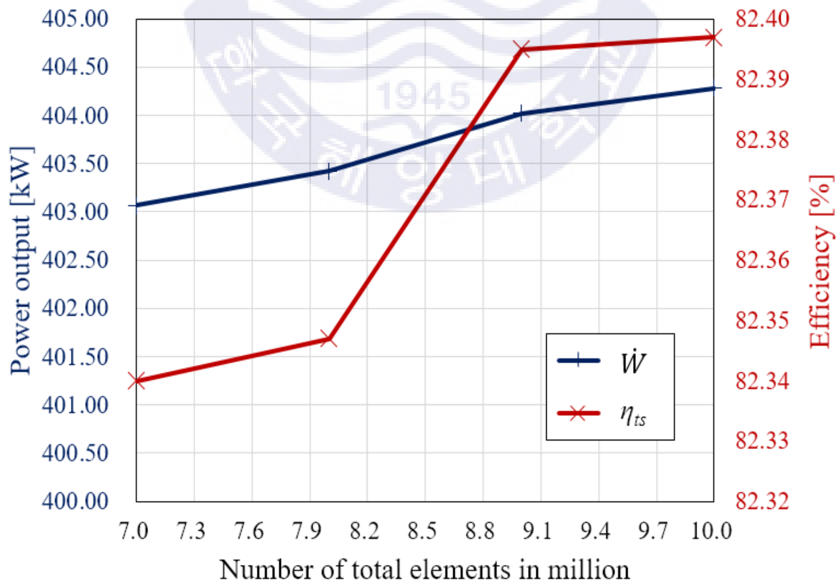

Fig. 35 Convergence test results of the final radial outflow turbine ($\dot{W}$ & η_{ts})

Table 16 Information of final grid

Domain	No. element	max. y+
Nozzle	4,406,380	23.489
Rotor	4,409,508	21.570

4.5.3 Final performance

Table 17 compares the design conditions and performance of the radial outflow turbine designed in this study. The CFD analysis results show that the performance of the radial outflow turbine designed is in good agreement with the design conditions.

Table 17 Performance of the radial outflow turbine

Parameters	Design values	CFD results
PR_{ts} [-]	1.47	1.44
TR_{ts} [-]	1.05	1.05
$\dot{W}$ [kW]	400.00	404.02
η_{ts} [%]	80.00	82.40

4.6 Performance analysis of off-design conditions

Off-design performance analysis was undertaken using various independent variables to understand off-design performance and to establish performance charts of the radial outflow turbine for an organic Rankine cycle. As per the previous case study, the independent variables considered in the off-design performance analysis were the turbine inlet temperature, mass flow rate, pressure ratio, and rotational speed.

Fig. 36 shows the power output and total-to-static efficiency according to the turbine inlet temperature and rotational speed. It was found that the power output increases in proportion to the inlet temperature of the turbine at each rotational speed. At the design RPM, the turbine efficiency continues to increase over the inlet temperature range of 393–423 K and decreases at 433 K. At other RPMs, the turbine efficiency changes rapidly with variations of the inlet temperature, with the exception of 90 % RPM.

Fig. 37 shows the power output and total-to-static efficiency according to the mass flow rate and rotational speed. M for the independent variable is the same as Eq. (27) in Section 3.6. The power output increases in proportion to the mass flow rate entering the turbine at each rotational speed. At the design RPM, the turbine efficiency continues to rise over the M range of 0.90 –1.10. At other RPMs, the turbine efficiency varies largely with changes in the mass flow rate, with the exception of 90 % RPM.

Fig. 38 shows the power output and total-to-static efficiency according to the pressure ratio and rotational speed. The power output increases in proportion to the pressure ratio at each rotational speed. Similar outputs are shown at the same pressure ratio regardless of the rotational speed. At the design RPM, the turbine efficiency continues to increase to a pressure ratio range of 1.50 and then decreases. At other RPMs, the turbine efficiency varies greatly according to changes in the pressure ratio, with the exception of 90 % RPM.

The off-design performance analysis of the radial outflow turbine for the organic Rankine cycle was similar to the tendency of the turbine for the supercritical CO_2 power cycle. Typically, the power output increases in proportion to the turbine inlet temperature, mass flow rate and pressure ratio. The turbine efficiency also showed a similar trend according to each independent variable. In other words, even in the turbine for the organic Rankine cycle, operating the turbine close to the design RPM could render high efficiency under various off-design conditions. Here, in the organic Rankine cycle turbine, the efficiency change was relatively small and the high efficiency range was maintained according to the change of each independent variable even at 90% RPM.

The difference between the supercritical CO_2 power cycle turbine and the organic Rankine cycle turbine is that the efficiency of the latter changes relatively rapidly in the independent variable change. The efficiency of the supercritical CO_2 power cycle turbine varies within 85.38−77.58 %, whereas the efficiency of the organic Rankine cycle turbine varies between 82.82−68.36 %. This indicates that the organic fluid is more sensitive to the operating conditions of the radial outflow turbine than the supercritical CO_2.

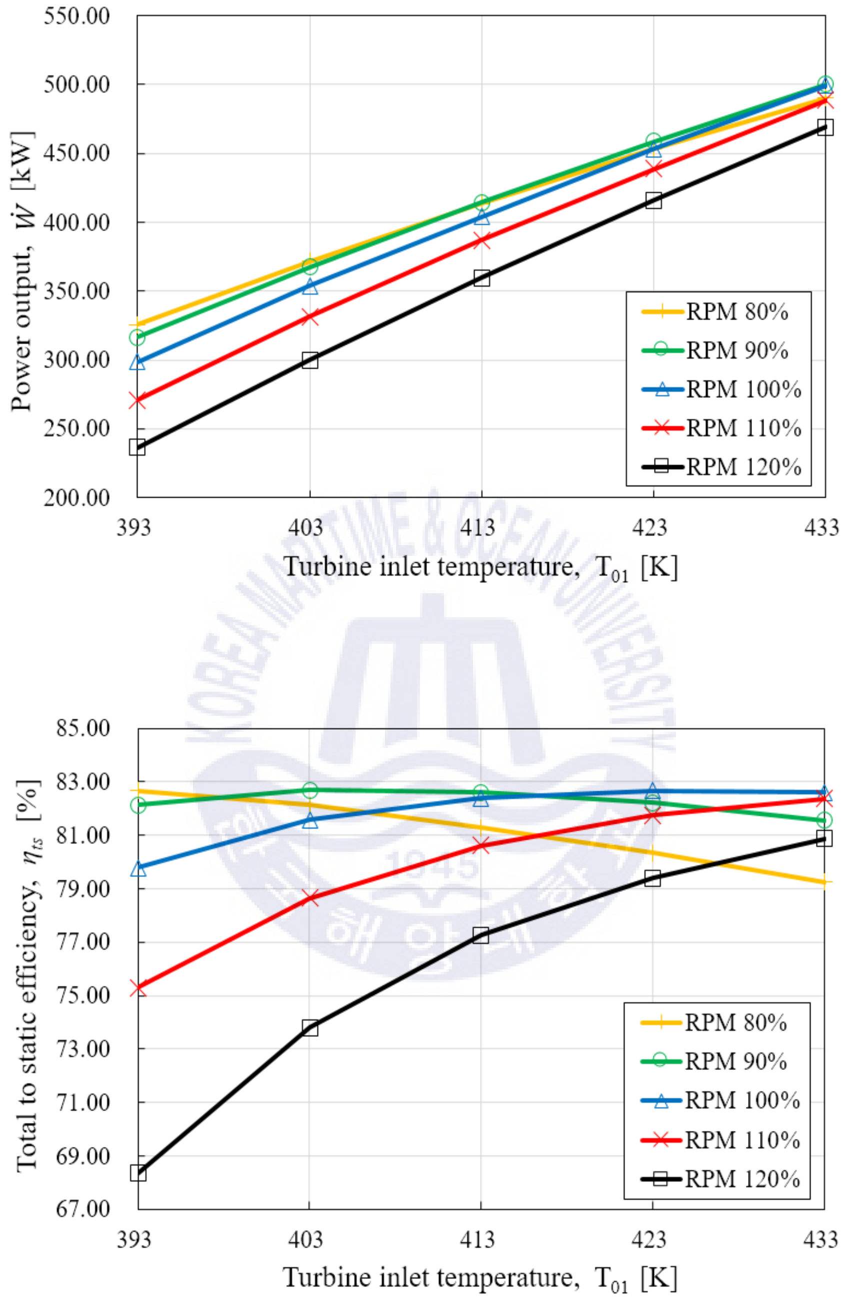

Fig. 36 Power output & total to static efficiency of the radial outflow turbine (T_{01} & RPM)

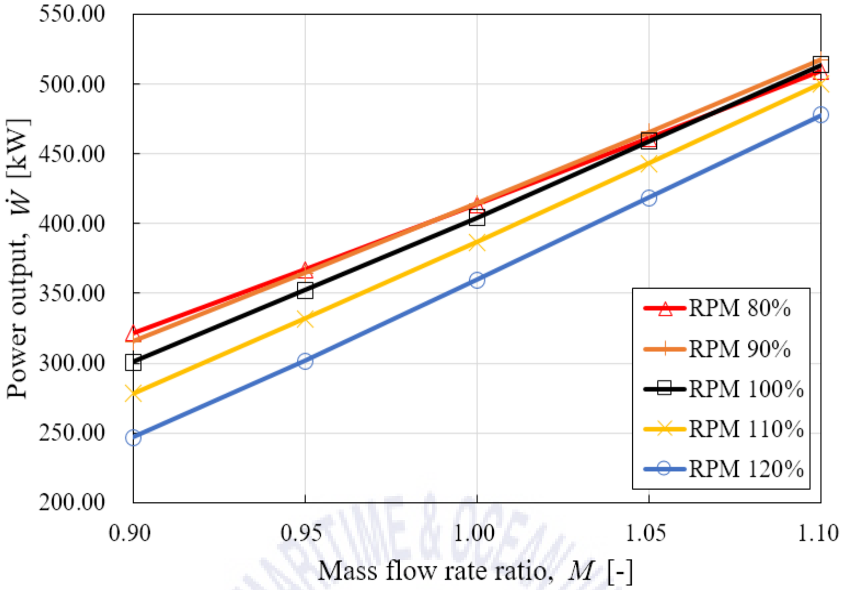

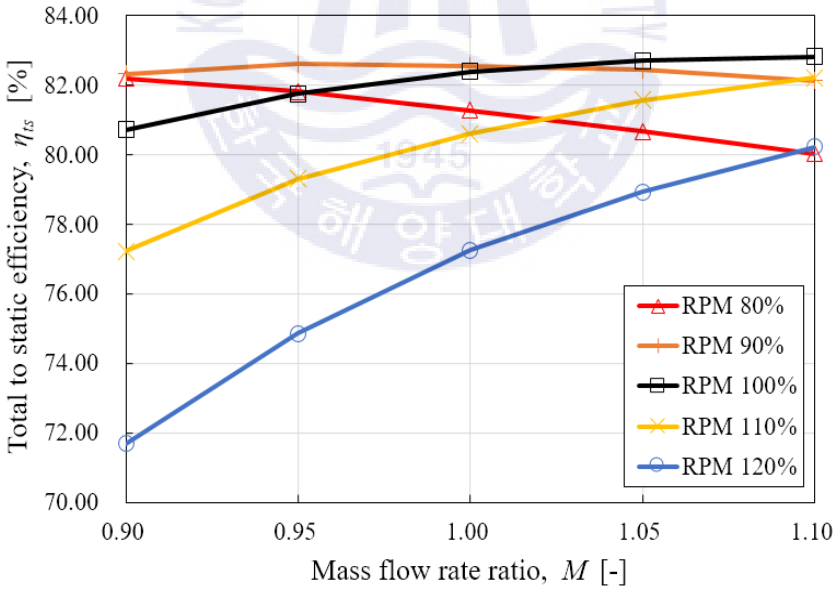

Fig. 37 Power output & total to static efficiency of the radial outflow turbine (M & RPM)

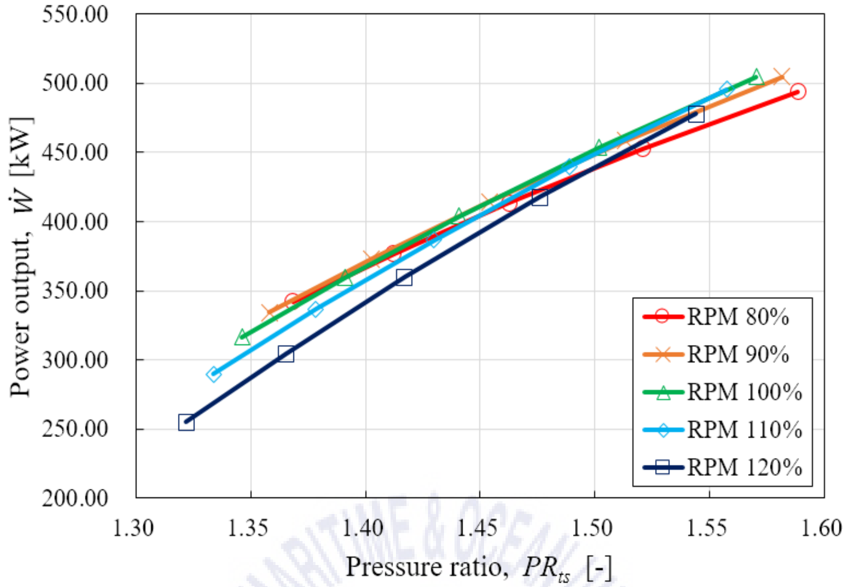

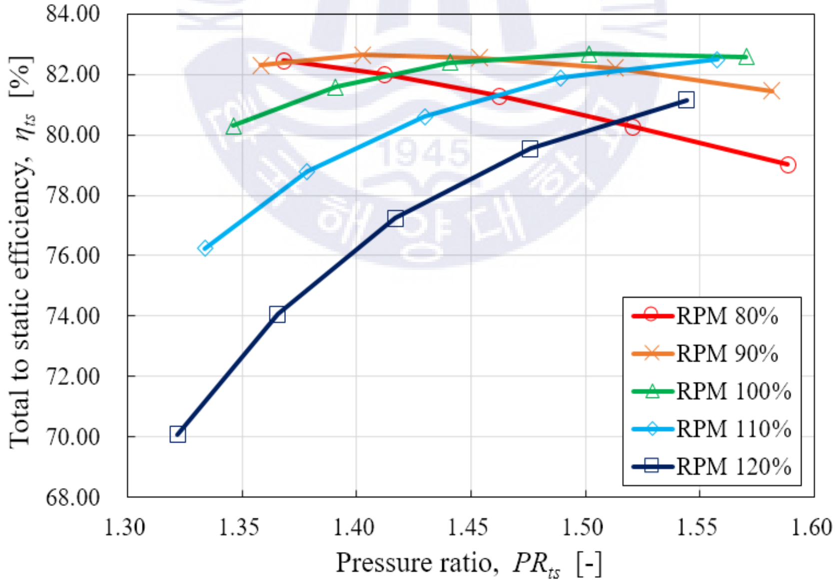

Fig. 38 Power output & total to static efficiency of the radial outflow turbine (PR_{ts} & RPM)

4.7 Performance curve based on dimensionless variables

4.7.1 Performance curve

Using the off-design performance results, the performance curves of the radial outflow turbine for the organic Rankine cycle according to the specific speed (N_s), loading coefficient (ψ), and flow coefficient (ϕ) are shown in Figs. 39–41.

Based on the performance curves of the turbine, there is a specific range of dimensionless variables that represent high efficiency. Therefore, if the value of each dimensionless variable is too high or too low, then it is unlikely to produce high turbine efficiency. The lowest point of turbine efficiency was approximately 68.36 % at the highest specific speed and the lowest loading and flow coefficients.

Table 18 shows the range of dimensionless variables that may produce a high efficiency of approximately 82.3 % or more in the turbine's performance curve. In the design of radial outflow turbines for organic Rankine cycles requiring high efficiency, the range of each dimensionless parameter given in Table 18 can be an important criterion in the determination of key design parameters.

In Figs. 39–41, each of A, B, and C is the same. Point A corresponds to the design point of the turbine and is in the high efficiency range. Points B and C are located at both ends of each performance curve and are in the relatively low efficiency range. Here, point C is the point of lowest efficiency in the performance curve. As per the previous case study, the CFD numerical analysis results were used to analyze the factors that influence the efficiency of the radial outflow turbine for an organic Rankine cycle.

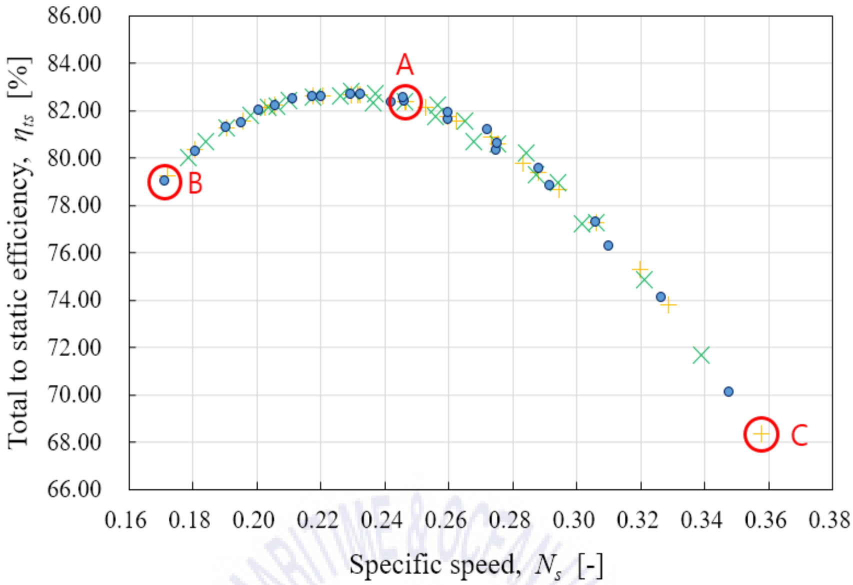

Fig. 39 Performance curve of the radial outflow turbine (N_s)

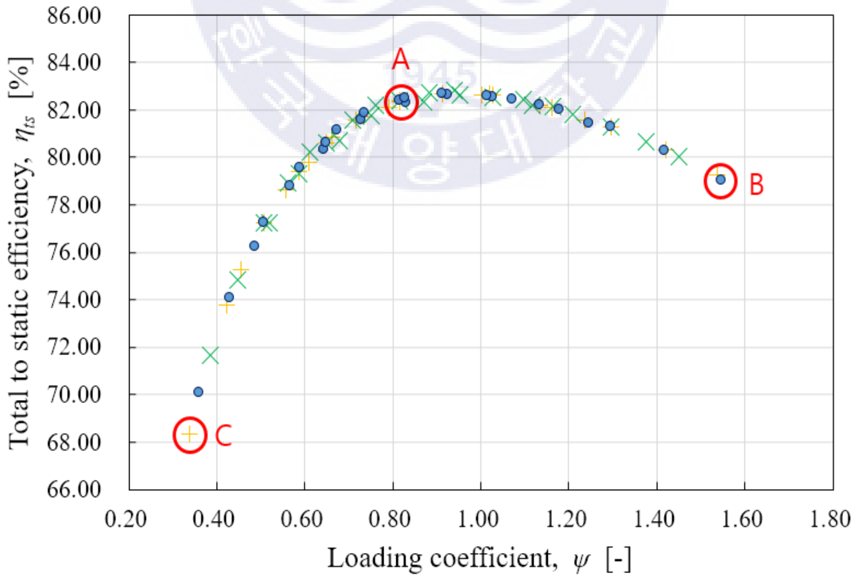

Fig. 40 Performance curve of the radial outflow turbine (ψ)

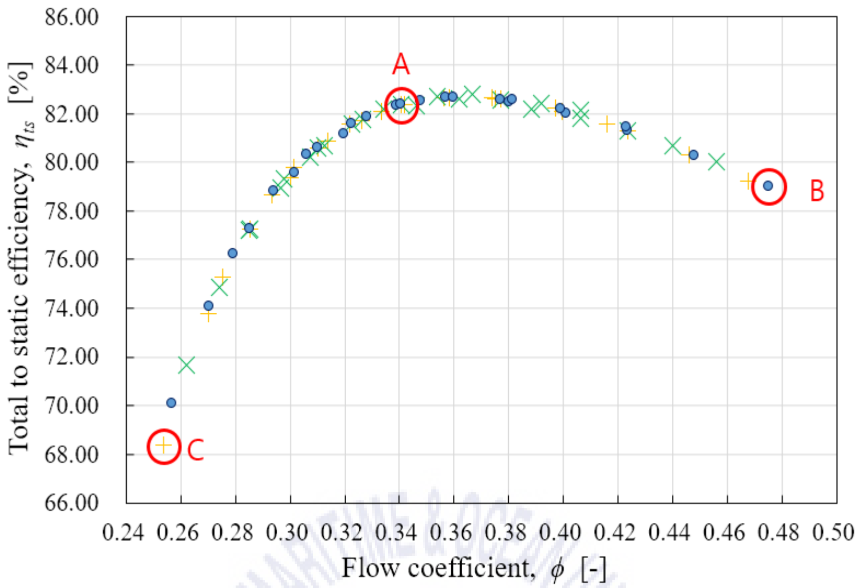

Fig. 41 Performance curve of the radial outflow turbine (ϕ)

Table 18 Range of dimensionless variables for high performance of the radial outflow turbine

Parameters	Range
Specific speed (N_s)	0.21 – 0.25
Loading coefficient (ψ)	0.80 – 1.10
Flow coefficient (ϕ)	0.34 – 0.39

4.7.2 Analysis of CFD results

Fig. 42 shows the static pressure contours for the three passages at points A, B, and C. As aforementioned, if the suction side has higher pressure than the pressure side of the rotor blades, then the rotation of the turbine is impeded. Looking at points A and B, the pressure decreases appropriately from the inlet of the nozzle blade to the exit of the rotor blade. In addition, the pressure side is always higher than the suction side in all areas of the rotor blades. At point C, the pressure decreases according to the flow direction, but there is a wide region where the pressure differential between the suction and the pressure sides is not apparent in the rotor blade. This may also cause the lowest efficiency in the turbine's performance curve. In term of the inlet pressure of the nozzle blade, the pressure at point C is lower than that of A and B. The pressure ratios of A, B, and C calculated by CFD are 1.44, 1.59, and 1.35, respectively.

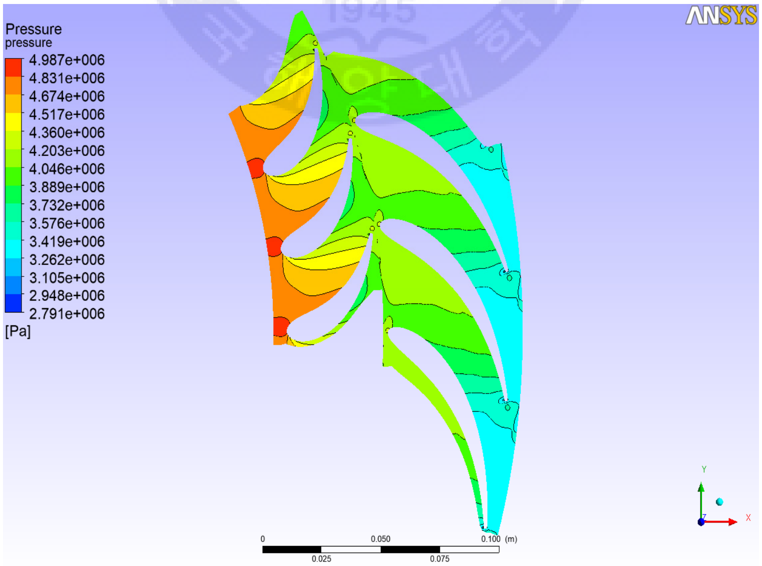

(A)

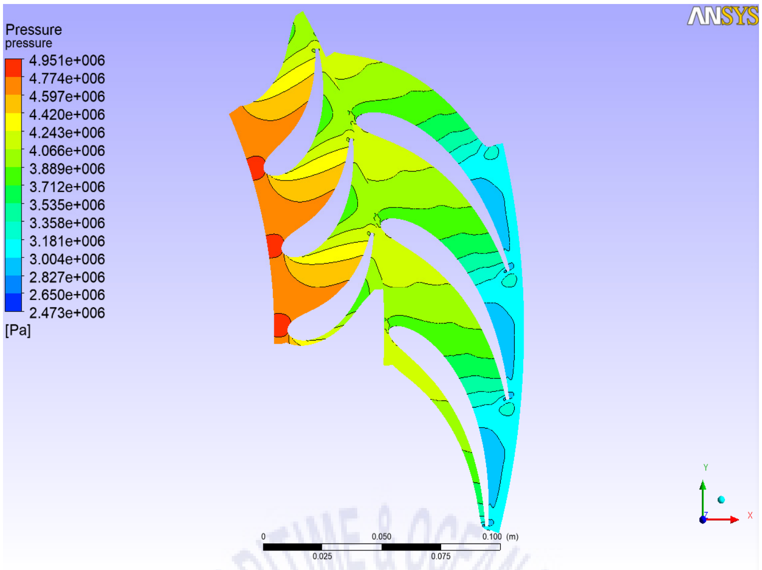

(B)

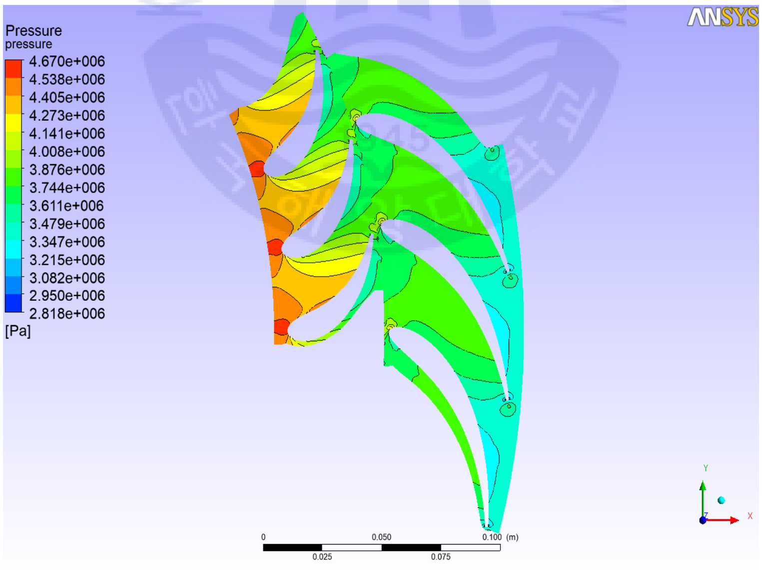

(C)

Fig. 42 Pressure contour of the radial outflow turbine

Fig. 43 shows the velocity contour at each point. As the fluid in the turbine expands from the inlet to the exit, the absolute velocity increases at the nozzle blades and the relative velocity increases at the rotor blades. As aforementioned, for the velocity contours it is necessary to look at the location of the stagnation point formed in the rotor blades. At point A, a small stagnation point is formed at the start of the leading edge of the rotor blade. At point B, the stagnation point is formed relatively wide on a certain pressure side on the leading edge of the rotor blade. At point C, a very small stagnation point appears on the suction side of the leading edge of the rotor blade. Compared with a supercritical CO_2 power cycle turbine, the size of each stagnation point is somewhat different, but the locations are similar. These results show that the flow characteristics at each point shown in the performance curves of the two radial outflow turbines are somewhat similar.

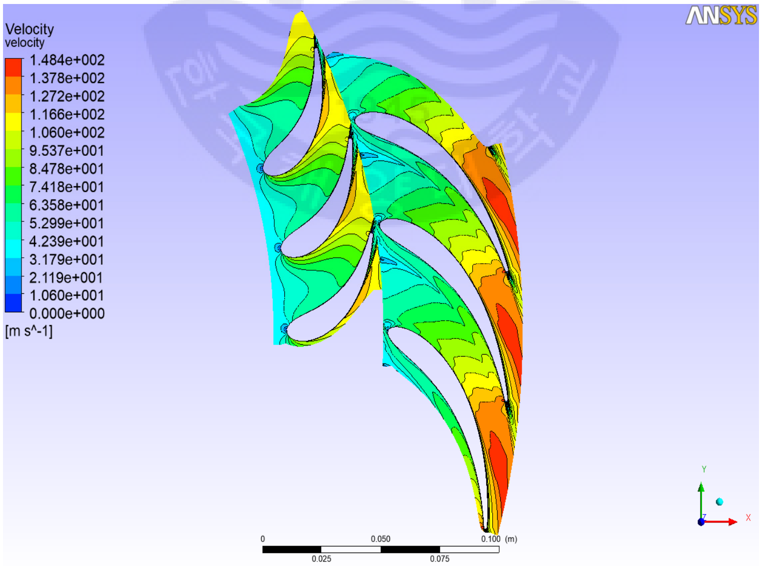

(A)

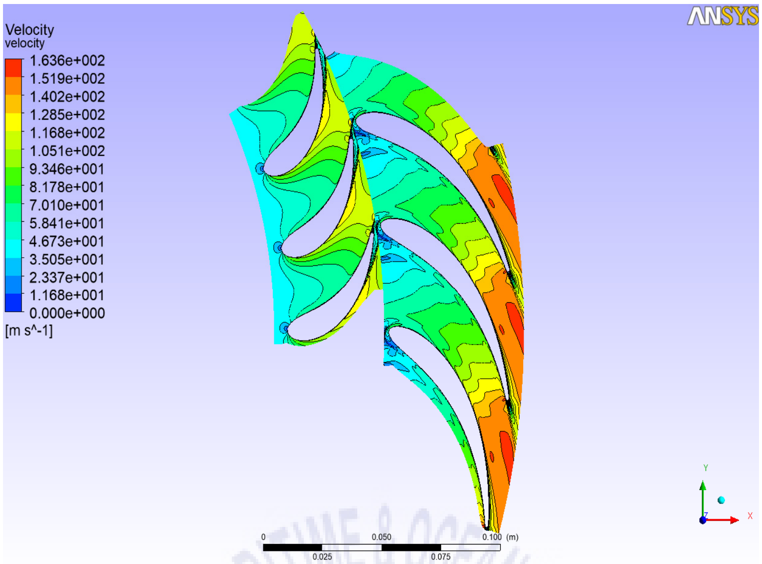

(B)

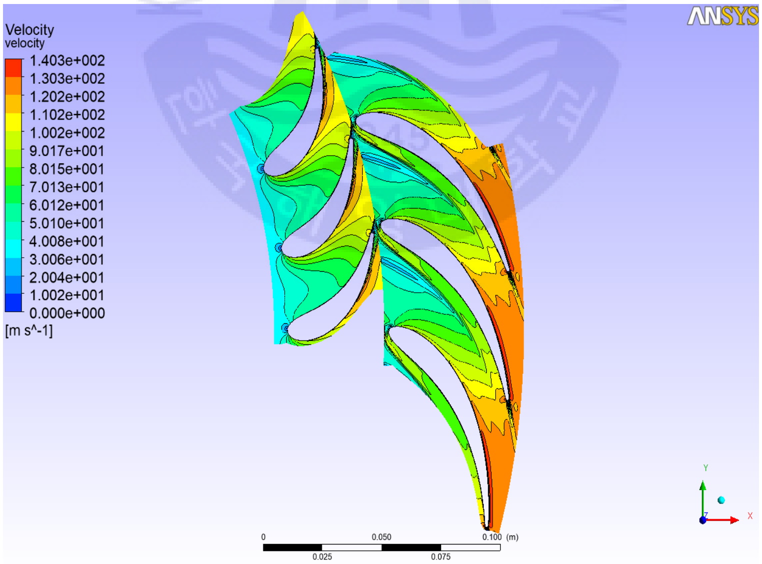

(C)

Fig. 43 Velocity contour of the radial outflow turbine

Fig. 44 shows the streamline at each point which differs at the leading edges of the rotor blades. At point A, a streamline is formed smoothly according to the shape of the rotor blade. At point B, the streamline is directed toward the pressure side at approximately 30.10° from the angle of the rotor blades (β_{2b}). At point C, the streamline is directed toward the suction side at approximately -20.85° from the angle of the rotor blades (β_{2b}). Looking at the difference between the angle of the rotor blade (β_{2b}) and the flow angle (β_2), the angle difference is larger at point B than at point C. Nevertheless, point C is the lowest point in the turbine's performance curve. This is confirmation that when the flow is overly directed to the suction side rather than to the pressure side of the rotor blades, an excessive reduction in turbine efficiency occurs. These results reinforce the findings from the previous case study.

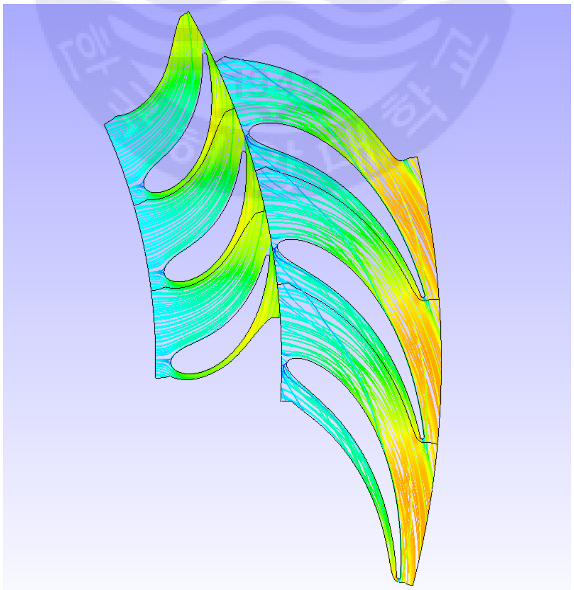

(A)

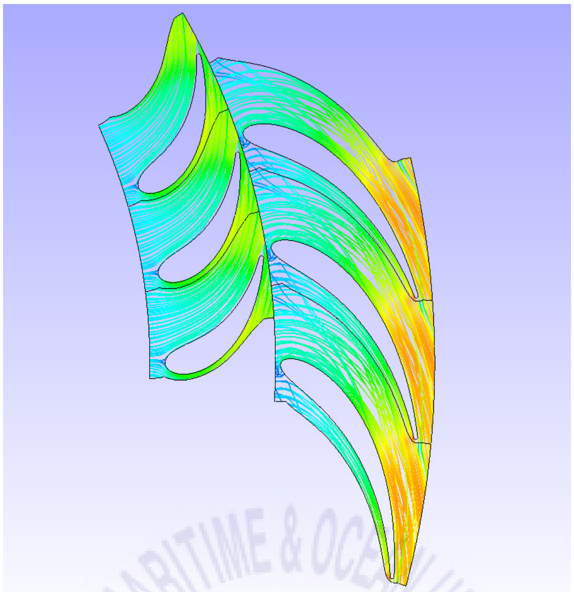

(B)

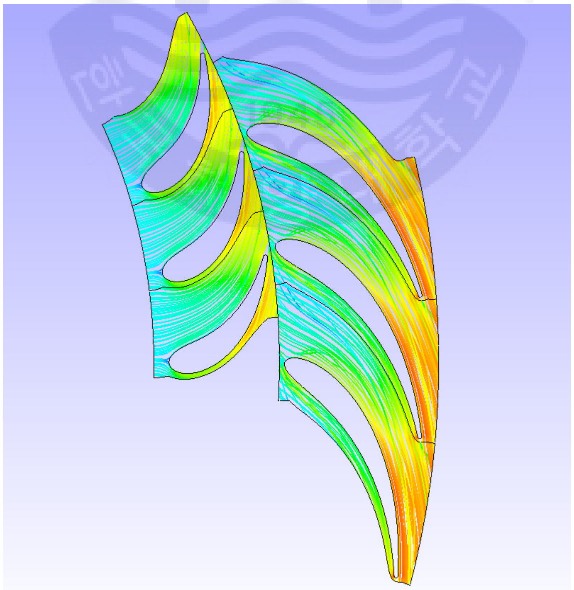

(C)

Fig. 44 Streamline of the radial outflow turbine

Chapter 5. Results and Discussion

In this study, a preliminary design program for radial outflow turbines was developed based on an algorithm using target efficiency as an input variable. The radial outflow turbines for the supercritical CO_2 power cycle and the organic Rankine cycle were designed through the developed preliminary design program. This chapter evaluates the preliminary design program based on the preliminary design and performance analysis of the turbine, summarizes the results and discusses the findings.

Table 19 shows the design conditions required for each cycle and the CFD results of the initial turbine shape presented by the preliminary design program. Both cycles showed that the CFD result had large errors with the design condition and did not meet the design goal. The causes of these errors and the subsequent results are discussed in this section. There is an absence of mathematical models of blade deviation angles for radial outflow turbines, which could not be reflected into the preliminary design program. However, the results of CFD analysis showed that deviation angles occurred from each blade, and the velocity triangle of each point presented in the preliminary design program could not be satisfied. Therefore, the initial turbine shape suggested by the preliminary design program requires optimization of the velocity triangle to meet the target performance.

When comparing the result values for the dimensionless variables of each turbine in Table 19, the specific speed (N_s) and loading coefficient (ψ) shows a large difference, but the value of the flow coefficient (ϕ) had a lower error rate. Based on these results, it is not appropriate to predict the performance of a turbine using only one dimensionless variable. Therefore, it is important to understand the efficiency of the turbine by considering the performance curves of specific velocity, loading and flow coefficients at the same time.

Table 20 shows the design conditions required for each cycle and the CFD results of the optimized turbine shape. In this study, only the nozzle exit angle and rotor inlet/exit angle were modified to optimize the velocity triangle. As a result, except for the efficiency of the supercritical CO_2 turbine, the error of each design condition is less than approximately 5 %. As turbine efficiency is somewhat higher due to the inherent problems of CFX, CFD results are in good agreement with the design conditions required for each cycle. Additionally, the specific speed (N_s), loading coefficient (ψ), and flow coefficient (ϕ) all had similar values for both results.

The developed preliminary design program for the radial outflow turbine can be evaluated using these two case studies. The preliminary design program suggests the shape of the turbine to meet the design requirements of the cycle. The initial shape of the turbine requires an optimization process due to the absence of a deviation angle model. This study proposed an optimization technique of the turbine using a systematic and easy method. This preliminary design program allows the design of radial outflow turbines that can sufficiently meet the target performance requirements of a supercritical CO_2 power cycle and an organic Rankine cycle, if the optimization technique is appropriately combined with the initial turbine shape.

Table 19 Performance of the initial radial outflow turbines in design condition

	Parameters	Design values	CFD results	Error
sCO_2 power cycle	PR_{ts} [-]	1.62	1.38	14.81 %
	TR_{ts} [-]	1.08	1.05	2.65 %
	$\dot{W}$ [MW]	10.00	6.50	35.04 %
	η_{ts} [%]	80.00	77.50	3.13 %
	N_s [-]	0.26	0.35	36.21 %
	ψ [-]	0.82	0.53	35.08 %
	ϕ [-]	0.35	0.36	2.12 %
Organic Rankine cycle (R143a)	PR_{ts} [-]	1.47	1.37	6.65 %
	TR_{ts} [-]	1.05	1.04	0.98 %
	$\dot{W}$ [kW]	400.00	333.38	16.66 %
	η_{ts} [%]	80.00	78.05	2.44 %
	N_s [-]	0.24	0.28	14.75 %
	ψ [-]	0.82	0.68	16.54 %
	ϕ [-]	0.35	0.35	0.43 %

Table 20 Performance of the optimized radial outflow turbines in design condition

	Parameters	Design values	CFD results	Error
sCO_2 power cycle	PR_{ts} [-]	1.62	1.62	0.42 %
	TR_{ts} [-]	1.08	1.07	0.19 %
	$\dot{W}$ [MW]	10.00	10.46	4.59 %
	η_{ts} [%]	80.00	85.30	6.63 %
	N_s [-]	0.26	0.26	1.22 %
	ψ [-]	0.82	0.85	4.02 %
	ϕ [-]	0.35	0.35	0.58 %
Organic Rankine cycle (R143a)	PR_{ts} [-]	1.47	1.44	2.03 %
	TR_{ts} [-]	1.05	1.05	0.24 %
	$\dot{W}$ [kW]	400.00	404.02	1.01 %
	η_{ts} [%]	80.00	82.40	2.99 %
	N_s [-]	0.24	0.25	2.64 %
	ψ [-]	0.82	0.82	0.06 %
	ϕ [-]	0.35	0.34	2.09 %

Table 21 summarizes the results for off-design analysis for radial outflow turbines for a supercritical CO_2 power cycle and an organic Rankine cycle. Points A, B, and C are the same as the points indicated in the performance curves according to the dimensionless variables discussed in Sections 3.7 and 4.7. In each cycle, the turbine's output is highest in B and lowest in C. Turbine efficiency is highest at design point A. Based on the CFD numerical results, the factors affecting the turbine efficiency can be identified through pressure distribution, the position of the stagnation point, and the streamline direction in the rotor blades. In Table 21, the dimensionless variables at each point clearly show different values, and the efficiency of the turbine in each cycle can be estimated according to the specific speed, loading and flow coefficients. When comparing two cycle turbines, the organic Rankine cycle turbine using R143a demonstrated greater efficiency change than the supercritical CO_2 power cycle turbine based on the change of operating conditions. In other words, the efficiency of the radial outflow turbine was found to be more sensitive to changes in operating conditions when using organic fluid than supercritical CO_2.

Figs. 45-47 depict the performance curves of the radial outflow turbine for each cycle according to specific speed, loading and flow coefficients. It should be noted that the range of dimensionless variables exhibiting high efficiency in each performance curve differs depending on the working fluid. There is a range of dimensionless variables where high efficiency is likely such as the area between the lines shown in Figs. 45-47. The range of dimensionless variables that can be used universally in the radial outflow turbine is summarized in Table 22. The table presented in this study, along with supercritical CO_2 and R143a, can be used to optimize the design of high efficiency radial outflow turbines.

Table 21 Performance of the radial outflow turbines in off-design condition

	Parameters	A	B	C
sCO_2 power cycle	PR_{ts} [-]	1.62	1.80	1.46
	TR_{ts} [-]	1.07	1.09	1.06
	M [-]	1.00	1.00	0.90
	RPM/RPM_{design} [-]	1.00	0.80	1.20
	$\dot{W}$ [MW]	10.46	11.98	6.69
	η_{ts} [%]	85.30	80.50	77.58
	N_s [-]	0.26	0.19	0.36
	ψ [-]	0.85	1.53	0.42
	ϕ [-]	0.35	0.47	0.26
Organic Rankine cycle (R143a)	PR_{ts} [-]	1.44	1.59	1.35
	TR_{ts} [-]	1.05	1.06	1.04
	M [-]	1.00	1.00	1.00
	RPM/RPM_{design} [-]	1.00	0.80	1.20
	$\dot{W}$ [kW]	404.02	493.68	236.64
	η_{ts} [%]	82.40	79.02	68.36
	N_s [-]	0.25	0.17	0.36
	ψ [-]	0.82	1.55	0.34
	ϕ [-]	0.34	0.48	0.25

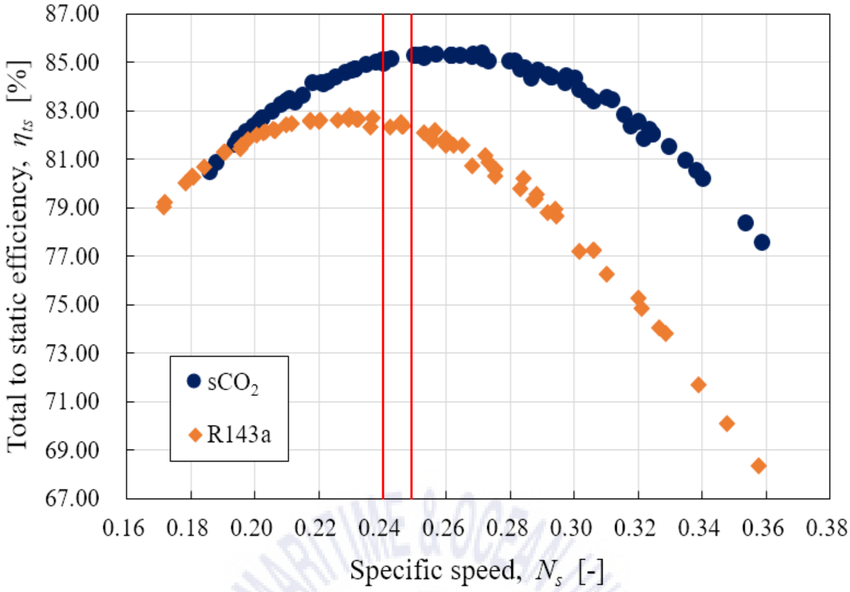

Fig. 45 Performance curve of the radial outflow turbines (N_s)

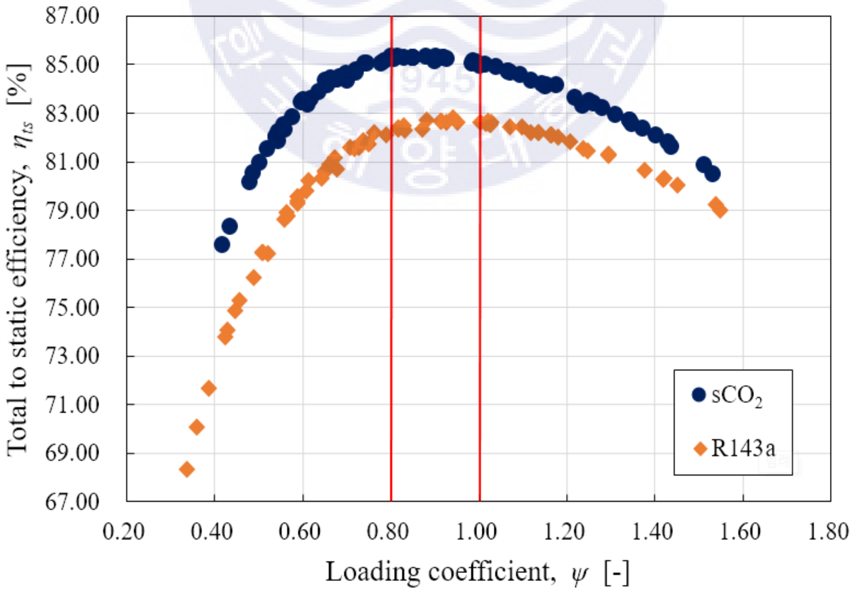

Fig. 46 Performance curve of the radial outflow turbines (ψ)

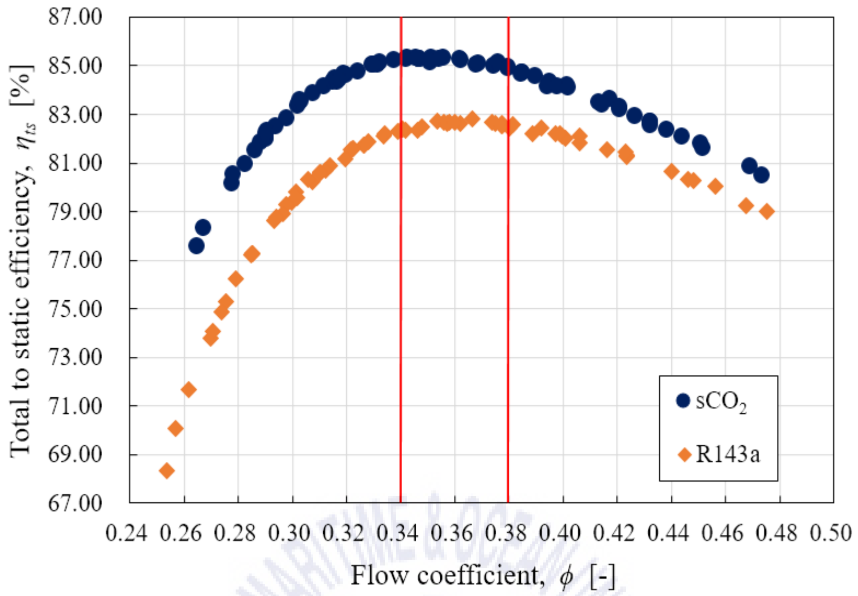

Fig. 47 Performance curve of the radial outflow turbines (ϕ)

Table 22 Range of dimensionless variables for high performance of the radial outflow turbines

Parameters	Range
Specific speed (N_s)	0.24 – 0.25
Loading coefficient (ψ)	0.80 – 1.00
Flow coefficient (ϕ)	0.34 – 0.38

Chapter 6. Conclusions

The supercritical CO_2 power cycle and the organic Rankine cycle are environmentally friendly cycles that can replace classic energy production systems that cause environmental pollution and global warming. Radial outflow turbine is a turbomachinery attracting attention from these fields of power generation. This study conducted the preliminary design and performance analysis of radial outflow turbines for the supercritical CO_2 power cycle and the organic Rankine cycle. The conclusions can be summarized as follows.

First, a preliminary design program for radial outflow turbines using a unique algorithm was developed. The main feature of the program is that the turbine can be designed to approximate the efficiency required by the cycle by using the target efficiency as an input to the program. This differs from the existing method that requires only the maximum efficiency of the turbine and can reduce the inefficient case of re-designing the cycle according to the designed turbine efficiency. The developed program is characterized by using pressure loss models at the core of the algorithm. Specifically, pressure loss models were used to determine the shape of the turbine and to accurately predict the quantity of state at the nozzle exit, greatly affecting efficiency. Turbine specifications were proposed for efficient design and easy fabrication, based on the assumptions specified in Section 2.2. The algorithm was also configured to perform iteration on only one variable. This means that the preliminary design program enables faster turbine design compared to preliminary design techniques that require iterative calculations for two or more variables.

Second, the preliminary design program demonstrated that it is possible to design radial outflow turbines for a supercritical CO_2 power cycle and an organic Rankine cycle. The initial shape of the turbine presented in the preliminary design program did not satisfy the design conditions. At present, there are few studies that point to the importance of the blade deviation angle in research associated with radial outflow turbines. However, this study found that the deviation angle of the blade is an important variable that greatly affects the performance of the turbine. The lack of mathematical deviation angle models for radial outflow turbines could not be reflected in the preliminary design step. This study proposed the optimization technique of radial outflow turbine by using a systematic and easy method for the initial shape of turbine. Specifically, the velocity triangle was optimized for the nozzle and rotor sequentially, and the design conditions were satisfied by only modifying the nozzle exit angle and rotor inlet/exit angle. The preliminary design program developed demonstrates that it is possible to design radial outflow turbines that satisfy the design conditions of each cycle through the initial shape of the turbine and the proposed optimization technique.

Third, I conducted off-design performance analysis of radial outflow turbines designed in each cycle. The performance analysis according to various off-design operation conditions demonstrated that turbine output was increased in proportion to the turbine inlet temperature, mass flow rate and pressure ratio. The turbine efficiency at the design RPM showed a small change according to variations in the independent variables and maintained a relatively high efficiency. This means operating the turbine to approach the design RPM is advantageous for the turbine's performance. Comparing the turbines in each cycle, the power and efficiency tended to be similar as the independent variables changed. The difference was that the organic Rankine cycle turbine changes efficiency more rapidly than the supercritical CO_2

power cycle turbine during independent variable changes of the same criteria. That is, the radial outflow turbines were found to be more sensitive to changes in operating conditions when using organic fluid than supercritical CO_2.

Fourth, I established performance curves according to specific speed, loading and flow coefficients. With the appropriate use of these dimensionless variables, it is possible to determine the main design parameters of a radial outflow turbine. At present, there are no performance curves of radial outflow turbines for the supercritical CO_2 and R143a according to the dimensionless variables. In this study, the performance curves of radial outflow turbines according to specific speed, loading and flow coefficients were proposed by using the off-design performance analysis results of each turbine. That is, the radial outflow turbine using supercritical CO_2 and R143a can predict the efficiency according to the specific speed, loading and flow coefficients by using the performance curves presented in this study. This study specified the high and low efficiency points in the performance curves according to the dimensionless variables. It also analyzed the CFD numerical results of each point to determine the factors affecting turbine efficiency. Specifically, when the suction side of the rotor blade has a higher pressure than the pressure side, the efficiency of the turbine is lowered by inhibiting the rotation of the rotor. In addition, there was relatively low efficiency when the stagnation point of the rotor blade appeared on the pressure side or suction side. The findings also demonstrated that if the inlet flow angle of the rotor is excessively directed to the suction side of the rotor blade, then the efficiency of the turbine is greatly reduced.

Finally, I proposed a universally optimal range of dimensionless variables for radial outflow turbines. Since the performance curves of specific speed, loading and flow coefficients differ depending on the working fluid, the range of dimensionless variables showing high efficiency is different. In this study, a common range for high efficiency could be found in the performance curves of each turbine. This study proposed a range of dimensionless variables that can be used universally for the optimal design of radial outflow turbines requiring high efficiency.

The preliminary design program for radial outflow turbines currently developed needs to study a broader variety of working fluids and cycle design conditions. The findings in this study are expected to be the cornerstone of design technology for radial outflow turbines that will be improved continuously. With steady ongoing research, the design technology of the turbine developed in this study can be gradually established in the fields of a supercritical CO_2 power cycle and an organic Rankine cycle.

References

Ahn, Y., Bae, S.J., Kim, M., Cho, S.K., Baik, S., Lee, J.I., & Cha, J.E., 2015. Review of supercritical CO_2 power cycle technology and current status of research and development. *Nuclear Engineering and Technology*, 47(6), pp.647–661.

Ainley, D. G., & Mathieson, G. C. R., 1951. A method of performance estimation for axial-flow turbines. *Aeronautical Research Council Reports and Memoranda*, No. 2974.

Al Jubori, A., Daabo, A., Al-Dadah, R.K., Mahmoud, S., & Ennil, A.B., 2016. Development of micro-scale axial and radial turbines for low-temperature heat source driven organic Rankine cycle. *Energy Conversion and Management*, 130, pp.141–155.

Al Jubori, A.M., Al-Dadah, R.K., & Mahmoud, S., 2017b. New performance maps for selecting suitable small-scale turbine configuration for low-power organic Rankine cycle applications. *Journal of Cleaner Production*, 161, pp.931–946.

Al Jubori, A.M., Al-dadah, R.K., Mahmoud, S., & Daabo, A., 2017a. Modelling and parametric analysis of small-scale axial and radial-outflow turbines for Organic Rankine Cycle applications. *Applied Energy*, 190, pp.981–996.

ANSYS, 2010. CFX Version 13.0 Modeling Guide.

ANSYS, 2010. CFX Version 13.0 Theory Guide.

Aungier, R.H., 2006. *Turbine Aerodynamics*. ASME Press.

Bao, J., & Zhao, L., 2013. A review of working fluid and expander selections for organic Rankine cycle. *Renewable and Sustainable Energy Reviews*, 24, pp.325–342.

Casati, E., Vitale, S., Pini, M., Persico, G., & Colonna, P., 2014. Centrifugal Turbines for Mini-Organic Rankine Cycle Power Systems. *Journal of Engineering for Gas Turbines and Power*, 136(12), 122607.

Cayer, E., Galanis, N., Desilets, M., Nesreddine, H., & Roy, P., 2009. Analysis of a carbon dioxide transcritical power cycle using a low temperature source. *Applied Energy*, 86, pp.1055–1063.

Cho, J., Shin, H., Ra, H.-S., Lee, G., Roh, C., Lee, B., & Baik Y.J., 2016. Development of the Supercritical Carbon Dioxide Power Cycle Experimental Loop in KIER. *Proceedings of ASME Turbo Expo 2016: Turbomachinery Technical Conference and Exposition*, GT2016-57460.

Choi, B.C., 2016. Thermodynamic analysis of a transcritical CO_2 heat recovery system with 2-stage reheat applied to cooling water of internal combustion engine for propulsion of the 6800 TEU container ship. *Energy*, 107, pp.532–541.

Da Lio, L., Manente, G., & Lazzaretto, A., 2014. New efficiency charts for the optimum design of axial flow turbines for organic Rankine cycles. *Energy*, 77, pp.447–459.

Dixon, S.L., 1998. *Fluid Mechanics and Thermodynamics of Machinery*. Elsevier.

Fuller, R., Preuss, J., & Noall, J., 2012. Turbomachinery for Supercritical CO_2 Power Cycles. *Proceedings of ASME Turbo Expo 2012*, GT2012-68735.

Iverson, B.D., Conboy, T.M., Pasch, J.J., & Kruizenga, A.M., 2013. Supercritical CO_2 Brayton cycles for solar-thermal energy. *Applied Energy*, 111, pp.957–970.

Kang, S.H., 2012. Design and experimental study of ORC (organic Rankine cycle) and radial turbine using R245fa working fluid. *Energy*, 41(1), pp.514–524.

Kim, D.Y., & Kim, Y.T., 2017a. Preliminary design and performance analysis of a radial inflow turbine for ocean thermal energy conversion. *Renewable Energy*, 106, pp.255–263.

Kim, D.Y., & Kim, Y.T., 2017b. Preliminary design and performance analysis of a radial inflow turbine for organic Rankine cycles. *Applied Thermal Engineering*, 120, pp.549–559.

Kim, J.S., Kim, D.Y., & Kim, Y.T., 2019. Fundamental design of a radial outflow turbine for a supercritical carbon dioxide power generation cycle. *International Symposium on Marine Engineering and Technology 2019*, BEXCO, Busan, Korea, October 24–25, 2019.

Kim, J.S., Kim, D.Y., & Kim, Y.T., 2019a. Thermodynamic analysis of a dual loop cycle coupled with a marine gas turbine for waste heat recovery system using low global warming potential working fluids. *Journal of Mechanical Science and Technology*, 33(7), pp.3531–3541.

Kim, J.S., Kim, D.Y., & Kim, Y.T., 2019b. Experiment on radial inflow turbines and performance prediction using deep neural network for the organic Rankine cycle. *Applied Thermal Engineering*, 149, pp.633–643.

Kim, J.S., Kim, Y.T., & Kim, D.Y., 2019. A fundamental study on the preliminary design of a radial outflow turbine. *Journal of the Korean Society of Marine Engineering*, 43(7), pp.535–544.

Kim, J.S., Yi, J.H., & Kim, Y.T., 2018. Thermodynamic Analysis and Optimization of a Transcritical Carbon Dioxide Rankine Cycle for Ocean Thermal Energy Conversion. *Transactions of the Korean Society of Mechanical Engineers - B*, 42(11), pp.721-733.

Kim, Y.M., Kim, C.G., & Favrat, D., 2012. Transcritical or supercritical CO_2 cycles using both low- and high-temperature heat sources. *Energy*, 43(1), pp.402-415.

Lee, J., Lee, J.I., Ahn, Y., & Yoon, H., 2012. Design Methodology of Supercritical CO_2 Brayton Cycle Turbomachineries. *Proceedings of ASME Turbo Expo 2012*, GT2012-68933.

Liu, Y., & Huang, D., 2019. Design and performance analysis of an ORC transonic centrifugal turbine. *Journal of Mechanical Science and Technology*, 33(3), pp.1417-1430.

Luo, D., Liu, Y., Sun, X., & Huang, D., 2017. The design and analysis of supercritical carbon dioxide centrifugal turbine. *Applied Thermal Engineering*, 127, pp.527-535.

Luo, D., Tan, X., & Huang, D., 2018. Design and performance analysis of three stage centrifugal turbine. *Applied Thermal Engineering*, 138, pp.740-749.

Maksiuta, D., Moroz, L., Burlaka, M., & Govoruschenko, Y., 2017. Study on applicability of radial-outflow turbine for 3 MW WHR organic Rankine cycle. *Energy Procedia*, 129, pp.293-300.

Mathworks, 2016. Matlab Version R2016a User Guide.

Meher-Homji, C.B., 2000. The historical evolution of turbomachinery, *Proceedings of the 29th Turbomachinery Symposium*, pp. 281-322.

Moustapha, H., Zelesky, M.F., Baines, N.C., & Japikse, D., 2003. *Axial and Radial Turbines*. Concepts NREC.

Nist, 2013. Refprop Version 9.1 User Guide.

Odabaee, M., Sauret, E., & Hooman, K., 2016. CFD Simulation of a Supercritical Carbon Dioxide Radial-Inflow Turbine, Comparing the Results of Using Real Gas Equation of Estate and Real Gas Property File. *Applied Mechanics and Materials*, 846, pp.85-90.

Persico, G., Dossena, V., & Gaetani, P., 2017. Optimal Aerodynamic Design of a Transonic Centrifugal Turbine Stage for Organic Rankine Cycle Applications. *Energy Procedia*, 129, pp.1093-1100.

Persico, G., Pini, M., Dossena, V., & Gaetani, P., 2013. Aerodynamics Design and Analysis of Centrifugal Turbine Cascades. *Proceedings of ASME Turbo Expo 2013: Turbine Technical Conference and Exposition*, GT2013-95770.

Persico, G., Pini, M., Dossena, V., & Gaetani, P., 2015. Aerodynamics of Centrifugal Turbine Cascades. *Journal of Engineering for Gas Turbines and Power*, 137(11), 112602.

Persico, G., Romei, A., Dossena, V., & Gaetani, P., 2018. Impact of shape-optimization on the unsteady aerodynamics and performance of a centrifugal turbine for ORC applications. *Energy*, 165, pp.2-11.

Pini, M., Persico, G., Casati, E., & Dossena, V., 2013. Preliminary Design of a Centrifugal Turbine for Organic Rankine Cycle Applications. *Journal of Engineering for Gas Turbines and Power*, 135(4), 042312.

Sarkar, J., 2015. Review and future trends of supercritical CO_2 Rankine cycle for low-grade heat conversion. *Renewable and Sustainable Energy Reviews*, 48, pp.434-451.

Sauret, E., & Gu, Y., 2014. Three-dimensional off-design numerical analysis of an organic Rankine cycle radial-inflow turbine. *Applied Energy*, 135, pp.202–211.

Sauret, E., & Rowlands, A.S., 2011. Candidate radial-inflow turbines and high-density working fluids for geothermal power systems. *Energy*, 36(7), pp.4460–4467.

Sayers, A.T., 1990. *Hydraulic and Compressible Flow Turbomachines*. McGraw-Hill.

Sharma, O.P., Kaushik, S.C., & Manjunath, K., 2017. Thermodynamic analysis and optimization of a supercritical CO_2 regenerative recompression Brayton cycle coupled with a marine gas turbine for shipboard waste heat recovery. *Thermal Science and Engineering Progress*, 3, pp.62–74.

Song, Y., Sun, X., & Huang, D., 2017. Preliminary design and performance analysis of a centrifugal turbine for Organic Rankine Cycle (ORC) applications. *Energy*, 140, pp.1239–1251.

Spadacini, C., & Rizzi, D., 2017. Radial outflow turbines for Organic Rankine Cycle expanders. Organic Rankine Cycle (ORC) Power Systems. pp.335–359.

Spadacini, C., Centemeri, L., Danieli, M., Rizzi, D., & Xodo, L., 2015. Geothermal Energy Exploitation with the Organic Radial Outflow Turbine. *World Geothermal Congress 2015*, pp.1–6.

Tartière, T., & Astolfi, M., 2017. A World Overview of the Organic Rankine Cycle Market. *Energy Procedia*, 129, pp.2–9.

Tchanche, B.F., Lambrinos, G., Frangoudakis, A., & Papadakis, G., 2011. Low-grade heat conversion into power using organic Rankine cycles – A review of various applications. *Renewable and Sustainable Energy Reviews*, 15(8), pp.3963–3979.

Tchanche, B.F., Pétrissans, M., & Papadakis, G., 2014. Heat resources and organic Rankine cycle machines. *Renewable and Sustainable Energy Reviews*, 39, pp.1185-1199.

Wang, J., Sun, Z., Dai, Y., & Ma, S., 2010. Parametric optimization design for supercritical CO_2 power cycle using genetic algorithm and artificial neural network. *Applied Energy*, 87(4), pp.1317-1324.

Wang, N., Sun, X., & Huang, D., 2019. Design and Analysis of a Single-Stage Transonic Centrifugal Turbine for organic Rankine cycle (ORC). *Journal of Thermal Science*, 27(2018).

Wang, Y., Tan, X., Wang, N., & Huang, D., 2018. Aerodynamic design and numerical study for centrifugal turbine with different shapes of volutes. *Applied Thermal Engineering*, 131, pp.472-485.

Zhang, X.R., Yamaguchi, H., Fujima, K., Enomoto, M., & Sawada, N., 2006. A feasibility study of CO_2-based Rankine cycle powered by solar energy. *JSME International Journal, Series B: Fluids and Thermal Engineering*, 48(3), pp.540-547.